INVESTIGATION OF CONSTRAINT EFFECTS ON FLAW GROWTH IN COMPOSITE LAMINATES

by

Peter Chun-Ngok Yeung

Dissertation submitted to the Graduate Faculty of the
Virginia Polytechnic Institute and State University
in partial fulfillment of the requirements for the degree of
DOCTOR OF PHILOSOPHY
in
Materials Engineering Science

APPROVED:

K. L. Reifsnider, Chairman

E. G. Henneke, II

W. W. Stinchcomb

C. W. Smith

J. E. McGrath

October, 1979

Blacksburg, Virginia

ACKNOWLEDGEMENTS

The author wishes to express his sincere appreciation to his major advisor, Dr. K. L. Reifsnider, for his guidance, support and encouragement during the course of this endeavor. He is also thankful to Dr. W. W. Stinchcomb for his continuing guidance throughout the investigation. Thanks as well go to Drs. E. G. Henneke, II and J. C. Duke, Jr. for their helpful suggestions and to Prof. C. W. Smith and Dr. J. E. McGrath for serving on his committee.

The financial support provided by NASA Langley under grant NSG-1364 is gratefully acknowledged.

Special thanks is extended to for her excellence in typing this dissertation.

The author also wishes to express his appreciation to

for his repeated willingness to help whenever called upon;

for doing some of the photographic work; and

for the assistance in the use of the graphics terminal.

The author also wishes to thank all the people he has had the opportunity to work with while at Virginia Tech, especially , , , , graduate students , , and . Their kindness and friendship and willingness to help has truly made the author's stay in Virginia a most enjoyable experience.

Lastly, but not least, the author wishes to thank his parents for their support and understanding throughout this endeavor. Their love and encouragement is what made it possible for his achieving his goal.

TABLE OF CONTENTS

TABLE OF CONTENTS
(Continued)

LIST OF FIGURES

LIST OF TABLES

I. INTRODUCTION

In recent years, advanced fiber reinforced composites have gradually emerged as a new class of engineering materials and have been gaining increasing acceptance in the engineering design of structural components. The desirable properties of high strength to weight and stiffness to weight ratios, together with the good fatigue resistance of composites to cyclic loading, have made composites strong candidate materials for many structural applications including aircraft, spacecraft and automobiles. The resulting demand for new design criteria and methodology have prompted an increasing interest for better understanding of the response of the material under various kinds of loading and service conditions.

In many of the applications, stress raisers such as notches, holes, slits, slots and other kinds of cutouts are purposely introduced in the material as required by design. Furthermore, inherent defects such as voids, fiber breakage, debond area, material nonuniformity and surface flaws can exist due to the fabrication and handling of the material alone. Since most composite materials are constructed by the lamination of various laminae of different orientations to achieve strength and stiffness in certain desired directions, the presence of such stress raisers and defects creates an extremely complex local situation as far as the stress state is concerned. One consequence of the complexity of local stresses is the complexity of damage that develops near a notch or flaw. Damage in composite materials may include a combination of fiber breakage, matrix cracking, fiber-matrix debonding, delamination and void growth, and the mechanism of damage and damage development depends upon

parameters such as material system, stacking sequences of plies, specimen geometry, stress state and environment. The response of a composite laminate under cyclic fatigue loading may also differ significantly and is generally more complex, when compared to the static response of the material.

A great amount of work has been conducted to study the fatigue behaviour of composite materials [1], but from an applications viewpoint, one of the most important and, yet, incompletely answered questions concerns the fatigue response of notched composite materials. It has been found that matrix crazing and cracking and debonding between reinforcing fibers frequently combine to produce "splitting" along the fiber directions near the tips of a notch [2-6]. Delamination in the interlaminar region is often observed at or near a notch or flaw and generally plays an important role in the fatigue damage development of composites [4,7-11]. The delamination may occur because of undamaged laminate stresses such as interlaminar normal stress, or it may be induced by damage. In most cases, delamination is not naturally arrested during cyclic loading. Some fiber breakage may occur in the vicinity of the notch when the applied load is high enough. Individual fiber breakage events are generally not evident except for certain cases of large fiber material [10]. In general, several of these damage modes are present at any given time prior to failure.

One of the major factors controlling the means by which fatigue damage progresses in composite laminates is the constraint imposed on one ply by its adjacent plies. By changing the stacking sequence of a laminate, one can alter the constraint imposed on a cracked ply in a

laminate, creating a different internal stress state which can significantly influence the crack growth and damage development in the laminate. Kendall had observed that the fatigue life of a $[90/0]_s$ laminate with a single-edge-notch was significantly less than that of a $[0/90]_s$ notched laminate [6]. Roderick and Whitcomb had found that by adding a 90° ply to a $[0/\pm45]_s$ B/Ep laminate, the principal damage regions around a center hole in the laminate were changed from a longitudinal orientation to a transverse orientation [10]. Grouping of 0° plies together in a laminate as opposed to interspersing the off-axis constraining plies tends to enhance the fiber splitting mode although the static strength of the laminate is increased [5,12]. In other cases, constraint effects by neighboring plies on a cracked ply served to blunt or arrest certain fatigue damage modes [3,13]. The nature of these constraint effects is, at present, poorly understood.

The analysis of the stress state around a notch or flaw in a composite laminate has not achieved complete success either. Most of the current approaches utilize the fracture mechanics viewpoint and include a damage zone near the crack tip [14]. The limited capability of such models to completely describe the notch situation in composites can be attributed to the facts that linear elastic fracture mechanics is not well suited to materials exhibiting heterogeneity on a scale comparable to the crack size and that a crack in a composite laminate seldom extends itself in a self-similar fashion. The mechanism by which damage in composites propagates is not well defined. Perhaps one of the contributing factors to this confusion, in addition to the nature of constraint effects, is the difficulty in nondestructively evaluating the

damage in composite materials accurately. Many different NDE techniques have been investigated for the purpose of detecting damage and damage growth in composite materials [15]. Some of the more commonly used techniques include ultrasonic c-scan [8], acoustic emission [16,17], and image enhanced X-ray [4,7,8,9]. In most cases, depending on the orientation and type of defect and damage, some techniques can be more applicable than others.

In the present study, the case of a transverse notch in an interior 0° ply or an interior 90° ply was investigated. Two constraint situations were examined: crossply and biaxial constraint. Throughout the investigation, various NDE techniques were used to follow the damage and damage development in the specimens. The objective of this study is to promote a better understanding of the nature of constraint effects on flaw growth in composite materials under cyclic loading. The results of this and other systematic studies of the response of composite materials will assist in the development of improved design criteria for composite structures.

II. APPROACH

2.1 Materials and Specimens.

The specimens used in this investigation were fabricated by Southwest Research Institute using T-300/5208 graphite epoxy prepreg tapes. Details of ply orientation and notch configuration for the specimens are given in Table 1. Specimen types 1 through 4 were 1.5 in. by 7 in. and types 5 and 6 were 1.5 in. by 10 in. The through-the-thickness notches were 0.25 in. long by 0.016 in. wide with a 0.008 in. radius at the notch tips. The notches were machined in the fabricated specimens using a 0.016 in. high speed diamond end mill.

Two types of constraint situations were examined, a cross-ply constraint where the orientation of the fibers in the constraining plies is perpendicular to the fiber orientation of the flawed plies (such as in type 3 and 4 specimens) and a biaxial constraint where ±45 degree plies are bonded to the flawed plies as in the type 5 and 6 specimens. Figures 1 and 2 show schematic diagrams of the ply orientations and notch configuration of the type 4 and 6 specimens, respectively.

The embedded notches in the types 3 through 6 specimens were through the center two plies of the laminates and were 0.25 in. long by 0.015 in. wide. These notches were made by milling the notch in the two prepreg plies simultaneously, filling the void with liquid silicone rubber (RTV-21) and curing. The silicone rubber filler has essentially no tensile or shear strength before and after cure.

2.2 Experimental Procedures

2.2.1 Mechanical Tests

All tests were run using a 20 Kip MTS testing machine operated in the load control mode. Load ranges were selected for maximum accuracy and reproducibility.

2.2.1.1 Static Tests

Three specimens of each type were subjected to static tension tests to determine the mean values of tensile strength, elastic modulus, and fracture strain. Strain data were obtained from strain gages and an extensometer attached to the specimens. Stacked strain rosettes were also attached to the through-the-thickness notched specimens at the notch tips to measure any localized response. Similar gages were mounted on the outside surfaces of specimens with embedded flaws above the tips of the interior flaws. The time resolved local behavior of the material in the neighborhood of the notch tips was recorded on video tape during the tests. Visual observations of response were made by re-playing the tape and noting the changes in the damage state during the test.

2.2.1.2 Fatigue Tests

The tension-tension fatigue tests were run at a stress ratio of $R = 0.1$ and a frequency of 10 Hz. The maximum cyclic stresses were selected using the static tensile strength values as a data base. A slow rate loading ramp was applied to bring the specimen to the desired mean load, and the elastic modulus was determined. A sinusoidal loading function of the desired amplitude was then superimposed on the mean load to

achieve a specific cyclic loading condition. The specimens were cycled at a constant maximum stress until fracture or 10^6 cycles, whichever occurred first. Typically, the test was interrupted at 1/2, 5×10^3, 1×10^4, 5×10^4, 1×10^5, 3×10^5 and 7×10^5 cycles to allow various nondestructive techniques to be applied to determine the damage development in the specimen.

2.2.2 Nondestructive Testing and Evaluation

A number of nondestructive investigative methods were employed before, during, and after the mechanical tests. These investigations were carried out in real time or with only short interruptions in the loading history. The objectives of these efforts were to measure the response of the material, to establish the nature of the damage state, and to determine the extent of damage in the material. The various techniques will be briefly outlined below. A more detailed description can be found in the references listed [15,18,19].

2.2.2.1 Replication

The method of replication was adapted to examine edge delaminations in composite laminates in earlier studies conducted at this university [19,20]. Cellulose acetate tape was softened with a diluted acetone solution and pressed against the surface where cracks are thought to exist. The tape flows into the surface detail and hardens. When the tape is removed, a record of the surface detail is obtained. The image on the tape can then be viewed in a microscope or reproduced on film for inspection. The replication process allows magnification of 50X to 100X without the depth of field limitations inherent to light microscopy so

that the method is actually preferable to direct observation using a standard microscope. Replicas were made at different load levels and/or different numbers of loading cycles. Replicas were also made of surfaces created by sectioning specimens which have undergone fatigue loading and have developed some damage. These replicas were used to document the damage in the vicinity of an embedded flaw.

2.2.2.2 Ultrasonic C-scan

The ultrasonic C-scan is a technique frequently used in the detection of planar defects, such as delaminations and voids, in composite laminates. Here, an ultrasonic pulse wave is transmitted through the test specimens using water as the transmitting medium. The returning echo from a support plate is gated and the amplitude of the signal is used to interpret the degree of damage in the laminate. All instrument settings were kept constant and a standard aluminum test piece with several known flaw sizes and configurations was used for calibration purposes to eliminate possible error due to the operation of the equipment. The output of the gated signal was controlled by a pre-set trigger level and was generally displayed on a grey-white area plot with the defective regions represented by white areas on the plot. The C-scan was used to determine the initial condition of the specimens and to follow the development of damage from an interior flaw constrained by outer plies during the fatigue testing of the specimens.

2.2.2.3 Ultrasonic Attenuation

A modification of the ultrasonic pulse-echo method was used to measure the attenuation in thin composite laminates, using a buffer block

for time resolution of the echos. When cracks form in a lamina under the ultrasonic transducer, the plane wave is scattered by the cracks, affecting the intensity of the returning echo. An analysis of the path followed by the echoes in the specimen and buffer block indicates that the measured changes in ultrasonic attenuation can be accounted for by diffraction or scattering effects caused by the developing damage state in the material [21,22]. A transducer placed directly above the flawed region of the specimen provided valuable information on the initiation and development of the damage around the interior flaw in the inner plies of the laminates.

2.2.2.4 Acoustic Emission

The damage mode in a composite laminate is a complex mechanism involving both fiber breakage, matrix cracking, and delamination between the individual plies. Any type of damage formation causes a sudden and localized change in the stress field around the damaged area, producing an emission of energy at the microscopic level. The emission is detected by an acoustical transducer, and amplified to yield a signal. Although it is difficult to interpret the acoustic emission data in terms of the discrete damage events, the technique proved itself to be a useful tool in detecting the onset of damage in composite materials.

2.2.2.5 X-Radiography

In order to use x-rays to successfully detect fatigue cracks in composite laminates, an image enhancement agent, such as tetrabromoethane (TBE) is generally required to make the damaged regions opaque to x-rays. In an attempt to eliminate the use of such toxic agents,

soft x-rays were directed at thin composite laminates. The x-rays were generated at 15 kVp for a duration of one to two minutes with a tube current of 2.25 mA continuous. The image was recorded on film, which was then processed for picture development. When an interior axial split developed in such a way that the plane of the matrix crack was aligned with the direction of travel of the x-rays, the soft x-rays gave a good indication of the extent of the cracking in the interior of the specimens.

2.2.2.6 Thermography

Fatigue crack initiation and damage growth in composite laminates can be readily followed by thermography [19,23]. Damage events in composites dissipate energy as heat which is picked up by an infrared camera with a ten-color isotherm display unit. The real-time display of the thermal image patterns of the specimen enabled one to directly assess the combined effect of the multiple damage modes which formed the damage state in the composite materials. By distinguishing between steady-state stress-field-related heat dissipation and transient heat development, it is possible to determine the severity of defect development and monitor the propagation and distribution of flaws in the specimens tested. The image patterns at various stages of the fatigue loading were recorded using a standard 35 mm camera.

2.2.2.7 Stiffness

The apparent global stiffness, as measured by an extensometer over the flawed region, gives another means of detecting the onset of flaw growth and the subsequent fatigue damage development in a composite

laminate. When the off-axis plies begin to fail in static loading, a knee or step develops in the stress-strain curve, reflecting a change in the stiffness of the material. This is usually accompanied by an increase in acoustic emission events together with an abrupt change in the ultrasonic attenuation value, giving a good indication of the beginning of the damage process.

In the fatigue studies, stiffness was also measured quasi-statically during the various cyclic intervals of the fatigue loading process. The change in the stiffness was then compared with the fatigue damage growth as observed by other nondestructive techniques. A severe damage growth was usually indicated by a significant drop in the global stiffness measured by the extensometer.

2.2.3 Sectioning Studies

In order to determine the extent of the internal damage around the embedded flaw, and to compare with results obtained by the nondestructive investigations, some specimens were sectioned and replicated.

Transverse sections were made by sawing the specimen just above the transverse axis of the flaw and polishing the cut surface at the flaw position. Figure 3 shows a schematic diagram of sectioning studies on a type 4 $[90/0]_S$ flawed laminate. After the initial cut was made, subsequent sections were made by cutting and polishing at locations above and below the horizontal axis. Replicas of the polished surface of the cross sections at the various locations were also made, resulting in a permanent record of the damage detail on the entire surface of the section. These could then be studied in a microscope or used later in

photographic reproductions of the surface detail illustrations.

2.3 Ply-Stress Analysis

In order to accurately assess the effect of the different constraining plies on a given flaw situation, a common loading parameter is needed so that the local behavior of different laminates can be compared under at least one identical condition. As a first attempt at identifying an appropriate parameter, the nominal stress in the flawed ply was selected. Specifically, the total loads to be applied to type 4 $([90/0]_s$ with an embedded flaw in the interior 0° plies) and type 6 $([\pm 45/0]_s$ with an embedded flaw in the interior 0° plies) specimens were calculated to produce the same nominal stress in the 0° plies in each laminate. These calculations were computed using laminated plate theory including the mechanical and thermal curing stresses.

The theory of laminated plate analysis has been well documented [24]. When a laminate is stressed, the resultant forces and moments acting on the laminate are obtained by integration of the stresses in each layer or lamina through the laminate thickness. The integration can be rearranged to take advantage of the fact that the stiffness matrix for a lamina is constant within the lamina, and with substitution of the lamina stress-strain relations, one can arrive at an expression relating the resultant forces (N) and moments (M) acting on a laminate to the middle surface strains (ε°) and curvatures (K) of the laminate.

$$\begin{Bmatrix} N_x \\ N_y \\ N_{xy} \end{Bmatrix} = \begin{bmatrix} A_{11} & A_{12} & A_{16} \\ A_{12} & A_{22} & A_{26} \\ A_{16} & A_{26} & A_{66} \end{bmatrix} \begin{Bmatrix} \varepsilon_x^\circ \\ \varepsilon_y^\circ \\ \gamma_{xy}^\circ \end{Bmatrix} + \begin{bmatrix} B_{11} & B_{12} & B_{26} \\ B_{12} & B_{22} & B_{26} \\ B_{16} & B_{26} & B_{66} \end{bmatrix} \begin{Bmatrix} K_x \\ K_y \\ K_{xy} \end{Bmatrix} \tag{1}$$

$$\begin{Bmatrix} M_x \\ M_y \\ M_{xy} \end{Bmatrix} = \begin{bmatrix} B_{11} & B_{12} & B_{16} \\ B_{12} & B_{22} & B_{26} \\ B_{16} & B_{26} & B_{66} \end{bmatrix} \begin{Bmatrix} \varepsilon_x^\circ \\ \varepsilon_y^\circ \\ \gamma_{xy}^\circ \end{Bmatrix} + \begin{bmatrix} D_{11} & D_{12} & D_{16} \\ D_{12} & D_{22} & D_{26} \\ D_{16} & D_{26} & D_{66} \end{bmatrix} \begin{Bmatrix} K_x \\ K_y \\ K_{xy} \end{Bmatrix}$$

where

$$A_{ij} = \sum_{k=1}^{N} (\overline{Q}_{ij})_k (Z_k - Z_{k-1})$$

$$B_{ij} = 1/2 \sum_{k=1}^{N} (\overline{Q}_{ij})_k (Z_k^2 - Z_{k-1}^2) \tag{2}$$

$$D_{ij} = 1/3 \sum_{k=1}^{N} (\overline{Q}_{ij})_k (Z_k^3 - Z_{k-1}^3)$$

The A_{ij} are called the extensional stiffnesses, the B_{ij} are called the coupling stiffnesses, and the D_{ij} are called the bending stiffnesses. The $\overline{Q}_{ij}$ are the transformed reduced stiffnesses and can be expressed in terms of the engineering constants of the material; Z_k denotes the distance from the midplane of the laminate to the interface between the k^{th} ply and the $k+1^{th}$ ply (Fig. 4). Eq. (1) can be rewritten in a simplified form as follows:

$$\left\{\begin{array}{c} N \\ \hline M \end{array}\right\} = \left[\begin{array}{c|c} A & B \\ \hline B & D \end{array}\right] \left\{\begin{array}{c} \varepsilon^\circ \\ \hline K \end{array}\right\} \tag{3}$$

Thermal-elastic Formulation:

Because of the anisotropy of the material, the thermal expansion coefficients in the principal directions of a lamina are quite different. Hence, when a laminate consisting of various plies of different fiber orientations is cooled from its curing stage, thermal residual stress develops within the plies.

The free thermal strain with temperature change, ΔT, from a strain-free temperature can be expressed as:

$$\{\varepsilon^T\} = \{\alpha\}\Delta T \tag{4}$$

where $\{\alpha\}$ are the thermal expansion coefficients of the material.

The total strain relationship is:

$$\{\varepsilon\} = \{\varepsilon^M\} + \{\varepsilon^T\} \tag{5}$$

where $\{\varepsilon^M\}$ is the mechanical strain and $\{\varepsilon^T\}$ is the thermal strain. The total strain can be expressed in terms of the middle surface strains (ε°) and curvatures (K) by:

$$\{\varepsilon\} = \{\varepsilon^\circ\} + Z\{K\} \tag{6}$$

To include the thermal effects in the laminated plate analysis, one can introduce an equivalent thermal force (N^T) and an equivalent thermal moment (M^T) and develop a modified version of Eq. (3).

$$\left\{\begin{array}{c} \overline{N} \\ \hline \overline{M} \end{array}\right\} = \left[\begin{array}{c|c} A & B \\ \hline B & D \end{array}\right] \left\{\begin{array}{c} \varepsilon^\circ \\ \hline K \end{array}\right\} \tag{7}$$

where $\{\overline{N}\} = \{N\} + \{N^T\}$

$$\text{and} \quad \{\overline{M}\} = \{M\} + \{M^T\} \tag{8}$$

$$\text{and} \quad \{N^T\} = \int_{-H}^{H} [\overline{Q}]^k \{\alpha\}^k \Delta T(z)\, dz$$

$$\{M^T\} = \int_{-H}^{H} [\overline{Q}]^k \{\alpha\}^k \Delta T(z)\, z dz \tag{9}$$

where H is the half-thickness of the laminate.

To develop an expression for the stresses in the k^{th} ply, we use Hooke's law and rewrite the mechanical stress-strain relationship as

$$\{\varepsilon^M\} = [S]\{\sigma\} \tag{10}$$

where [S] is the compliance matrix.

By rearranging terms and using Eqs. (4), (5) and (6), we get

$$\{\sigma\}^k = [\overline{Q}]^k (\{\varepsilon^\circ\} + Z^k \{K\} - \{\varepsilon^T\}^k) \tag{11}$$

where $\{\varepsilon^\circ\}$ and $\{K\}$ can be obtained by the inversion of Eq. (7).

Using the properties determined by the testing of the unnotched unidirectional lamina, as well as data supplied by the manufacturers of the specimens [18], we can obtain expressions for the axial stress in the interior 0° plies of the (1.5 inch wide) types 4 and 6 specimens:

$$\sigma_{x0^\circ} = 52.0P - 6.04 \text{ for } [90/0]_s \text{ laminates}$$

and (12)

$$\sigma_{x0^\circ} = 41.9P + 1.44 \text{ for } [\pm 45/0]_s \text{ laminates}$$

The stresses are in Ksi when the applied load, P, is in Kips.

Hence, for example, in order to produce nominal axial stress in the interior 0° plies for each laminate equal to 70 percent of the notched tensile strength of a unidirectional laminate (type 1 specimen), a $[90/0]_s$ laminate must be stressed to 36 percent of its ultimate tensile

strength (UTS) whereas a $[\pm 45/0]_s$ laminate must be stressed to 41 percent of its tensile strength.

III. RESULTS

3.1 Static Tension Tests

A summary of the static tensile strength data is listed in Table 2. All the notched $[90]_6$ specimens (type 2) failed transverse to the load axis through the notch region. However, in the presence of a constraint, embedded cracks in the 90° plies of the type 3 and type 5 specimens had little or no consequence in the final fracture process. The response of these laminates under static loading closely resembled that of the unflawed specimens, and, in many cases, the specimen did not break at the notch region.

During the testing of the type 3 $[0/90]_s$ flawed laminates, the test was interrupted at various load levels and edge replicas were made of the specimen. Transverse cracks at the free edge were observed in the 90° plies between 24 and 45 Ksi and these increased in density with increasing load No delamination between the plies was detected near the free edge. The final fracture was transverse, and in only one of the three specimens tested was the transverse fracture through the embedded flaw region.

In the case of the type 5 $[\pm 45/90]_s$ flawed laminates, transverse cracks, as well as small edge delaminations, were observed in the 90° plies as the load was being applied. These edge delaminations grew along the length of the specimen with increasing load and interacted with the transverse cracks by jogging between the -45/90 interfaces. As the applied stress approached the ultimate strength of the laminate, the delamination began to propagate into the width of the specimen. The final fracture was transverse but did not occur through the embedded

flaw location. The location of the final fracture coincided with initially defective regions away from the embedded flaw position as detected by ultrasonic c-scans of the specimens made before testing. These regions were probably regions of delaminations between the 90° and the ±45° plies, causing a relaxation of the constraint afforded by the normal bonding of these layers. The fracture in the interior 90° plies was parallel to the fibers with local delaminations of the -45/90 interfaces. The 45° fibers failed irregularly across the width of the specimen with local delaminations in the ±45° interfaces.

When the transverse flaw was placed in the 0° plies, the influence of the flaw on the static response of the material was more pronounced compared to the flawed 90° ply case. In the unconstrained case, axial cracks initiated at the notch tips of the transversely notched $[0]_6$ (type 1) specimens as matrix cracks at approximately 25 percent of the failure load. These cracks then extended along the fiber direction and propagated towards the ends of the specimens as the load was increased. The final failure was usually associated with the complete separation of the specimen into two parts along the longitudinal cracks which developed.

The response of a similarly notched lamina when constrained by unflawed laminae on both sides was quite different. In the case of a type 4 specimen where the constraining plies were 90° plies, transverse cracks in the exterior 90° plies were observed to develop at the notch location at stresses of approximately 20 Ksi (138 MPa) and grow to a length slightly longer than the notch at 45 Ksi (310 MPa). Between 40 Ksi (276 MPa) and 70 Ksi (483 MPa), surface creases in the 90° plies above and below the notch were observed where cracks developed at the

notch tips in the interior 0° plies and extended parallel to the fibers.

Figure 5 shows the ultrasonic attenuation measured across the flawed region for a type 4 specimen while being quasi-statically loaded to failure. Superimposed on the same diagram are the acoustic emission (A.E.) rate and longitudinal strain variations during the loading sequence. The strain gage was mounted approximately one half inch below the flaw location. (Fig. 6 shows a schematic diagram of the apparatus set-up.) Significant acoustic emission was detected when the remote stress reached a value of approximately 37 Ksi (255 MPa), and continued thereafter until fracture. At about the same stress level, the stress-strain behavior as measured by the remote strain gage began to deviate from linearity, and this was accompanied by a sudden change in the ultrasonic attenuation measurement across the flaw location. Since this is above the stress level at which the 90° plies began to separate at the flaw location, we can assume that the acoustic emissions detected are not entirely due to the cracking of the 90° plies. The sudden increase in attenuation measurement over the embedded flaw, however, suggests that axial cracks might be developing at the tips of the notch along the fiber direction in the interior 0° plies. The existance of these cracks relaxes the stress state in the region, causing a relaxation of strain measured by a remote gage mounted on the outer 90° plies in the region of the ligament. Hence, the presence of the constraining 90° plies provides additional transverse stiffness to the interior 0° plies, increasing the stress level at which these axial cracks develop when compared to the unconstrained case (type 1 specimens).

The stress level at which the A.E. rate begins to increase was

repeatable over several tests and remained approximately the same for tests without the ultrasonic attenuation transducer where the restraint from the positioning and clamping of the transducer directly above the flaw is eliminated. The final failure mode of the type 4 specimens was a transverse fracture of 0° plies initiating at the axial internal cracks (Fig. 7).

When a biaxial state of constraint was imposed on transversely notched 0° plies, such as in the case of type 6 specimens where the constraining plies were oriented at ±45°, the response of the laminate was significantly different. Figure 8 shows a typical plot of the variation of the measured parameters for a $[\pm 45/0]_s$ flawed laminate under monotonic loading. There were occasional bursts of A.E., but the pattern was not consistent. The stress-strain behavior was linear until just before fracture. The attenuation across the flawed region continuously increased for this specimen with increasing load. Fractures of these specimens were through the embedded flaw with the failure of the 0° plies extending away from the notch tip at 45° to the fiber direction. The remaining portion of the specimen failed transverse to the loading direction. Splitting of internal 0° plies at the notch tip was detected in some cases, but did not act as a major part of the static fracture.

3.2 Fatigue Tests

In the case of the through-thickness notched $[90]_6$ specimens, fatigue failure occurred through the notch parallel to the fiber direction when cycled at a maximum stress of over 55 percent of the

static tensile strength. For specimens which survived 10^6 cycles of fatigue loading, no visible damage was observed at the notch tips. It was suspected that as soon as a crack was initiated at the notch tip, catastrophic failure occurred with the crack running towards the edge of the specimen.

When the notched unidirectional 90° laminae are constrained by unflawed plies, the fatigue response of the type 3 and type 5 laminates is generally (embedded) flaw insensitive. At sufficiently high stresses, replicas at the free edge indicated the development of transverse cracks in the interior 90° plies of these laminates. The density of the cracks increased with increasing maximum cyclic stress and increasing cycles of fatigue loading. In some cases, the embedded notch in the 90° plies did not propagate out towards the free edge although transverse cracks were developing elsewhere. The transverse crack at the notch position in the interior 90° plies had little influence on the damage development and the final failure of the laminates.

When the maximum cyclic stress was increased to 80 percent of the ultimate tensile strength (UTS) of the laminate, the fatigue damage mode of a $[0/90]_s$ flawed laminate (type 3) developed into a more complicated form. In addition to the formation of the transverse cracks in the 90° plies, portions of the outer 0° plies began to separate from the 90° plies near the tips of the embedded notch as early as 17,000 cycles. The separation occurred over a width of approximately 1/16 inch and propagated along the loading direction towards the grips. Figure 9 shows the c-scan history of the specimen. The gated c-scan echo was triggered with respect to the top surface of the specimen. When the

ultrasonic wave scanned across the separated top surface of the specimen, the electronic gate was displaced in time with respect to the echo. Hence the damaged (white) region gave an approximation to the location and extent of these separations of the outer 0° plies on the top surface. The specimen failed in fatigue at 51,000 cycles. The fracture was transverse and away from the notch position, with portions of the 0° plies peeling off from the interior 90° plies at the fracture location.

For a $[\pm 45/90]_s$ flawed laminate (type 5) edge delaminations developed in the 90° plies and at the -45°/90° and ±45° interfaces when fatigued at high enough stresses because of the tensile interlaminar normal stress present at the free edge. These delaminations then propagated along the length and through the width of the specimen and dominated the fatigue damage growth in these laminates. No visible damage was detected around the embedded flaw region either by ultrasonic c-scan or thermography. Edge replicas indicated that there were some transverse cracks in the 90° plies. During the fatigue loading, a significant amount of heat was generated by the rubbing of the delaminated surfaces, with the localized temperature rise reaching 4°C, as detected by the thermographic camera. Final fracture occurred when the nondelaminated section of the specimen could no longer support the load applied. Figure 10 shows the c-scan of a type 5 specimen after 88,000 cycles of fatigue loading at a maximum stress equal to 61 percent UTS of the laminate. The major delamination had propagated over the half-width of the specimen with minor regions of delamination along the edges. There was no observable damage growth around the embedded flaw and the specimen failed shortly after.

Fatigue damage of the transversely notched $[0]_6$ (type 1) specimens initiated at the notch tips and propagated parallel to the fibers in an "H" pattern. The distance over which these axial cracks travelled varied in length, depending on the maximum load applied. For instance, when a type 1 specimen was cycled at a maximum stress amplitude of 50 percent of its static strength, axial splits developed at the crack tips as early as 2230 cycles, growing to approximately 1/2 inch in length by 3500 cycles. After 12,400 cycles of fatigue loading, the cracks had propagated to the gripped section. At high stresses, the cracks could propagate into the gripped region, causing a pull-out of the ligaments from the grips and a longitudinal failure. The crack initiation and growth during the fatigue loading could be easily followed by thermography (Fig. 11) although the hottest spot usually lagged slightly behind the tip of the crack.

A constrained notched 0° ply, such as in type 4 and type 6 specimens, presents a more complicated situation. Here, the embedded notch in the laminate becomes the source of damage development and depending on the orientation of the constraining plies, the interlaminar stresses influence the spread of damage in a complex way since the local stress field in the neighborhood of the flaw is extremely complex.

To accurately assess the effect of the different constraining plies on this flaw situation, the nominal stress in the flawed ply was selected as a common loading parameter. Specifically, the total applied loads required to produce the same nominal axial stress in the 0° plies of type 4 and type 6 specimens were calculated using equation 12. The stresses were generally expressed as percentages of the notched strength

of the type 1 specimens in comparing the results obtained.

3.2.1 C-Scan Results

C-scan histories of specimens with embedded flaws (in the interior 0° plies) are presented in Figs. 12-16. The c-scans were made at the cyclic intervals shown in the figures. In all figures, the horizontal arrow locates the position of the embedded flaw.

Figure 12 shows the development of damage as revealed by c-scans of a type 4 $[90/0]_s$ specimen after 100k, 300k, and 700k cycles at an applied stress equaled to 36 percent of UTS. By 100k cycles, an "H" pattern had formed at the flaw. Sectioning studies showed that the damage consisted of axial cracks at the tips of the notch in the 0° plies and delamination of the 90/0 interface. This will be described in greater detail later in the chapter. In addition, transverse cracks in the 90° constraining plies were also present. Additional cycles at this stress level caused the damage zone to grow in the transverse direction. Between 300k and 700k cycles, the c-scan reveals little or no growth of the damage zone. All c-scans were made by gating on the same echo and using the same sensitivity so that the size of the defective zones in different c-scans could be directly compared and used as a relative measure of the size of the damge zone detectable by the ultrasonic c-scan technique.

Higher applied stresses produced higher damage zone growth rates and larger damage zones. Figure 13 shows that the damage zone in a type 4 $[90/0]_s$ specimen at 51 percent of UTS continued to grow in the axial direction during the first 100k cycles where the test was stopped and

the specimen was sectioned. However, the transverse growth of the damage zone stopped after 5k cycles. Thermographs recorded during this test show "H" shaped hot spots as early as 1k cycles. Figure 14 shows that after 100k cycles at 70 percent UTS, the damage had extended to the grips in the axial direction and additional cycling to 300k cycles increased the extent of the damage in the transverse direction. By 300k cycles, the 90/0 interfaces had delaminated to the extent that the 90° plies no longer were effective constraining plies and the test was stopped. Visual inspection showed that the four axial cracks extending from the notch tips in the 0° plies had grown into the grip region creating a "no load" strip of unidirectional material above and below the embedded flaw and two load carrying strips on each side of the flaw.

Damage zones in type 6 $[\pm 45/0]_s$ laminates are shown in Figs. 15 and 16. The c-scans in Fig. 15 show the defective region around an embedded flaw in a specimen cycled at a maximum stress of 41 percent UTS. By 100k cycles, a damage zone had developed in the flawed region; however, there appeared to be little or no growth of the zone after 310k cycles. During this test, the thermographic camera detected a hot spot as early as 3.3k cycles, although the thermographic pattern was not as distinct as in the type 4 laminates.

Increasing the applied stress to 63 percent UTS created a larger damage zone after 100k cycles than cycling at 41 percent UTS (Fig. 16). The higher stress also caused the damage zone to increase in size between 50k and 100k cycles. The thermographs recorded a hot spot in the flawed region by 1.1k cycles.

3.2.2 Thermography

Fatigue damage development around the embedded flaw in the type 4 and type 6 laminates could be readily monitored in real time by thermography. The fatigue loading process created a friction between separated surfaces in the material, generating heat that was detected by the infrared camera. Figures 17 and 18 show the history of heat patterns generated during the fatigue testing of a type 4 and type 6 laminate respectively. In both cases, the specimens were loaded to a stress level at which the axial stress being applied to the flawed interior 0° plies was 130 percent of the notched strength of the type 1 laminates.

For the $[90/0]_s$ flawed laminate, hot spots near the embedded flaw could be detected as early as 540 cycles. By the time the maximum load was reached, the "H" shaped damage pattern was well established. As more cycles of fatigue were applied, the damaged area grew in size both along the axial and the transverse directions. The temperature difference between the hot spot and the remote regions of the specimen reached 7°C by 10k cycles with very little change thereafter. The damage was severe with axial splits at the notch tips in the interior 0° plies running all the way to the grips accompanied by delamination of the 90/0 interfaces. The specimen, however, survived a million cycles of fatigue loading and was later pulled for residual strength determination.

The heat pattern generated for the $[\pm 45/0]_s$ flawed laminate was not as clearly defined. A localized hot spot was detected after 500 cycles of initial loading. The temperature rise of the hot spot reached 2°C at 1590 cycles when maximum load was reached, and continued to increase

steadily. There was no observable directional preference in the damage development pattern, but the hot spot continued to grow in size and the temperature difference reached 6°C after 8200 cycles. The specimen failed in fatigue after 8750 cycles of loading. The localized temperature rise of the hot spot near the embedded flaw position in the specimen reached 10°C just before fracture. The fracture was transverse and passed through the embedded flaw with some degree of ligament pull-out.

3.2.3 Stiffness

The percent change in the apparent stiffness measured by a clip gauge across the embedded flaw region of the specimens could be used as a qualitative means of estimating the damage growth in the laminates. Although some inconsistency in the stiffness measurement might arise due to the method of attachment of the clip gauge, certain trends in the material property could be observed. Figures 19 and 20 show the changes in the apparent stiffness of the $[90/0]_s$ and the $[\pm 45/0]_s$ flawed laminates, respectively. In both cases, the percent change depended upon the cyclic stress amplitude and the number of cycles of fatigue loading, which governed the damage present and the growth of damage under cyclic loading. For specimens where the c-scans indicated a larger degree of delamination, there was usually a more significant decrease in the apparent stiffness measured at the corresponding life-cycle.

3.3 Sectioning Studies

The results discussed in earlier sections indicated that when a transverse flaw was introduced in an interior 0° ply of a laminate, the static and fatigue response of the laminate could be greatly influenced

by the presence of the flaw. The damage in the type 4 and type 6 specimens was a complex mechanism, involving axial splitting in the interior 0° plies, delamination at the ply interfaces, and matrix cracking in the off-axis plies. To understand the interaction between the various damage modes, one must first be able to determine the extent of the damage itself. Throughout this investigation, attempts were made to achieve this objective nondestructively. To assist the interpretation of the results obtained by the NDE tests, sectioning studies were made on several specimens of each type.

Reproductions of a series of section replicas made on a $[\pm 45/0]_s$ flawed laminate are shown in Fig. 21. The specimen had been fatigued at a stress level equal to 85 percent of the ultimate tensile strength of the laminate for 200,000 cycles before being sectioned. The X = 0 replica shows the transverse section through the embedded flaw. The arrows indicate the flaw position with respect to the width of the specimen. The fatigue damage of the type 6 specimen consists of delamination of the +45/-45 and the -45/0 interfaces, axial cracks along the fiber direction in the ±45° plies near the damage area, and axial splits originating at the tip of the flaw and running along the fiber direction in the interior 0° plies. The length of the axial splits and the extent of the delaminations were measured on the replicas and original photomicrographs, and the results are presented in Fig. 22. The figures are constructed with the aid of a Tektronix 4051 computer-graphics system.

To assist in the interpretation of the data, the results are presented for (A), delamination of the +45/-45 interface; (B), delamination of the upper -45/0 interface; (C), delamination of the lower 0/-45

interface; (D), delamination of the lower 45/+45 interface; and (E), a combined drawing showing the maximum extent of delamination in a 2-dimensional plane view and the length of the axial splits in the interior 0° plies. The transverse lines indicate the extent of delamination as measured from the replica made at that particular sectioning location. The vertical lines in Fig. 22E show the length of the axial splits in the interior 0° plies and suggest that these axial cracks are confined to the damaged region around the flaw and do not extend beyond the delaminated zone. The c-scan of the same specimen after 200,000 cycles is shown in Fig. 22F, and the shape and size of the delaminated region described by the sectioning data correlate well with the c-scan result.

Similar studies were conducted on the $[90/0]_s$ flawed laminates. Figures 23 and 24 show results for a type 4 specimen after 100,000 cycles of fatigue loading at 51% UTS maximum stress. Damage in the specimen included transverse cracking and peeling of the 90° plies, delamination of the 90/0 interfaces, and axial cracking of the interior 0° plies at the notch tips. When the extent of the damage was measured and reconstructed alongside the ultrasonic c-scan of the specimen (Fig. 24), it was found that the axial splits at the tips of the embedded flaw in the interior 0° plies had propagated beyond the delaminated region. The delaminated area correlated well with the c-scan diagram. Since the ultrasonic c-scan is more sensitive to planar type defects perpendicular to the direction of travel of the sound wave, the orientation of the axial splits creates difficulty for the c-scan technique to successfully detect such defects.

3.3.1 X-Ray Results

An alternative nondestructive technique used to determine the extent of the axial cracks in the interior plies was X-ray examination. When the crack plane was aligned with the photon beam, X-ray images provided an accurate measurement of the length of these cracks [25]. Figure 25 shows the X-ray and c-scan history of a type 4 specimen after 100k cycles of fatigue loading. The maximum nominal stress in the 0° plies was 100 percent of the notch strength of the type 1 specimens. The arrows in the diagram indicate the tips of the axial splits as detected by the X-ray patterns. In all cases, the extent of the splitting exceeded the delaminated area shown by the c-scans, although the general shapes of the damaged region correlated well with one another. Some effects of slight misalignment of the test specimen with the loading axis during the testing could be observed from the anti-symmetric form of the "H" shaped damage pattern developed. A longer axial crack length was accompanied by a greater area of delamination.

As for the $[\pm 45/0]_s$ flawed laminates, the tendency to form axial cracks at the interior notch tips was less than for the $[90/0]_s$ flawed laminates. However, some variation was noted due to initial quality of the specimen. When the cyclic stresses were low, there was no indication of axial cracking as detected by the X-rays although the c-scan diagrams showed some increase in the damaged zone due to the fatigue loading. At higher stresses, some cracking might develop at the tips of the interior notch. Figure 26 shows the X-ray and c-scan diagrams of a type 6 specimen after one million cycles of fatigue loading as compared to the original state. The maximum cyclic stress applied to the interior 0°

plies was 120 percent of the notched strength of the type 1 specimens. The extent of the axial cracks was confined within the delaminated zone agreeing with results obtained from the sectioning studies. Tilting of the specimen was required to produce a better image when the crack plane was not aligned with the direction of the X-ray beam.

3.4 Residual Strength

In the previous sections, the discussion of the fatigue damage in the transversely flawed laminates (type 4 and type 6 specimens) was usually described in terms of three measurable parameters: namely, the extent of axial cracking in the interior 0° plies; the degree of delamination at the interfaces; and the decrease in the apparent stiffness in the global section of the flawed region. Depending on the severity of the damage, the damage state in the specimens after undergoing fatigue loading could affect residual strength and the failure modes. Table III lists the residual strength data for some of the specimens which had undergone various cycles of fatigue loading at some predetermined cyclic stress amplitude, such that the extent of fatigue damage in these specimens was distinctly different. For instance, for the type 4 specimens, in specimen number 4, the damage in the laminate was severe, with the axial cracks at the flaw tips running all the way into the grip region and massive delamination along the axial cracks. Specimen number 2 contained only a small degree of axial splitting with some localized delamination. The damage in specimen number 3 was similar to that of number 2, but the extent of the internal axial cracks was longer.

When these specimens were pulled for residual strength after cyclic

loading, there was very little difference in the final fracture mode. The failure mode was a transverse fracture with some degree of axial cracking in the interior 0° plies both at the tips of the flaw and in the remote region, and was quite similar to the static failure mode of the specimens which had not undergone cyclic loading. There was no apparent difference in the residual strengths of these specimens, and in all cases, the net section stress in the interior 0° plies at fracture exceeded the measured strength of the unnotched unidirectional 0° laminates of 142 Ksi. In the case of specimen number 4, the constraint imposed by the 90° plies was partially relieved due to the extensive delamination present at the 90/0 interface. The degree of axial splitting was more severe and there was evidence of multiple transverse fractures in the 0° plies, resulting in a higher strength value.

Similar results were obtained from the type 6 specimens. When compared to the crossply constraint, there was a greater tendency for the biaxial constraining plies to restrict the spread of the fatigue damage when the nominal stress in the interior 0° plies of the laminates were equal. Higher cyclic stresses produced a larger area of damaged zone, although the shapes of the damaged region were essentially the same. When the interply delaminations had progressed to the extent of relaxing the constraint imposed on the flawed 0° plies, axial splits then developed at the notch roots in the interior plies. This would result in a slight change in the failure mode of the $[\pm 45/0]_s$ flawed laminates, producing a more transverse failure with some degree of ligament pull-out in the 0° plies. Such was the case for specimen number 1.

The fabrication of the specimens could also create a significant variation in the results of the testing. For the new type 6 specimens, an excessive amount of silicone rubber was introduced into the embedded notch during the lay-up process and was squeezed into -45/0 interface when the specimens were cured. This created a small region of unbonded surfaces near the flaw location as could be detected by X-ray and c-scan techniques. When the specimen was stressed, the presence of these unbonded regions caused a relaxation of the constraint effects on flaw growth, promoting the tendency for the formation of axial splits at the interior notch roots. The fracture of specimen numbers 2 and 3 of the type 6 laminates both contained 0° fiber failure running at 45° from the loading direction and emanating from splits at the notch tips. The net section stress at failure in the 0° plies (for the type 6 laminates) was lower than the average static value and the strength of the unnotched unidirectional 0° specimens suggesting that the influence of the notch was still present.

IV. DISCUSSION

The general objective of this investigation was to achieve an understanding of constraint effects for a well controlled set of circumstances. Results presented thus far were for the case when a transverse flaw was placed in an interior ply perpendicular to the loading axis. Two orientations of the flawed ply were examined: 0° flawed ply (embedded flaw perpendicular to the fiber orientation) and 90° flawed ply (embedded flaw parallel to the fiber orientation). The approach used consisted of evaluating constraint effects as they influenced the behavior of the flawed plies. The response of the unconstrained through-the-thickness-notched unidirectional lamina was first determined, and the effect of adding various angle plies to the flawed lamina was then treated as the "constraint effect." Throughout the investigation, two distinctly different constraining cases were being studied, a cross-ply constraint where the orientation of the constraining plies was at right angles to the fiber orientation of the flawed plies, and a biaxial constraint where ±45° plies were bonded to the flawed interior plies.

Because of the large number of possible variables that could be introduced into a composite laminate, some of the observations made could certainly not be applied to every constraint situation encountered by modern day composite structures. By independently changing the orientation of the flawed plies, or the configuration of the flaw, or the orientation of the constraining plies, one could significantly alter the response of the material and obtain a completely different set of results. Hence, the results being discussed here are, in some cases, only applicable to the particular constraint situation addressed.

However, certain trends and concepts, more general in nature, could be developed to assist in the understanding of the nature of constraint effects in a given situation.

Constraint effects, as described above, can generally be classified into two catagories: in-plane effects and through-the-thickness effects. The in-plane effects are those which act in the plane of the laminae and laminate, namely the (x,y) plane, and the through-the-thickness effects act across the thickness dimension in the (x,z) plane. The manner in which these two types of constraint effects influence the material behavior is quite different. However, both are effects resulting from the mismatch of properties by the coupling of laminae of different orientations in a laminate due to the anisotropic nature of fiber reinforced composite materials. When a flawed laminate is stressed, there may be effects which are directly related to the influence of the notch on the local situation in addition to the effect of lamination on damage development independent of the presence of the notch.

Results for specimens with flawed interior 90° plies indicated that no observable effect on the embedded flaw growth in the specimens resulted from imposing different orientations of the constraining plies. In fact, the presence of the embedded flaw had very little influence on the overall response of these laminates due to the limited load-carrying capacity of the 90° plies. The damage development in the types 3 and 5 specimens closely resembled that of the unflawed laminates. In the static and fatigue testing of the $[0/90]_s$ flawed laminates, transverse cracking of the 90° plies near the free edge could be detected from the edge replicas made. The spacing of the transverse

cracks decreased with increasing load and with increasing cycles of fatigue. Figure 27 shows the transverse crack development history of some of the type 3 specimens tested. The number of cracks in the 90° plies was counted over a one-inch length along the edge of the specimen, and the crack count was averaged over the two edges. Transverse cracks began to appear during the static preload at approximately 2000 lbs. load. The rate of increase of the transverse crack formation during the fatigue loading differed for the different specimens, with the specimen with the lowest cyclic maximum stress (55% UTS) showing the greatest rate of increase during fatigue. The specimen cycled at a maximum stress of 80 percent UTS had only a slight increase in crack count during the fatigue testing, but because of the high preload stress applied, the number of cracks present after 1/2 cycle was much greater than that of the other specimens.

In all cases, the crack count seemed to approach a saturation level as the fatigue loading process continued. This, combined with observations made on unflawed specimens and laminates of other stacking sequences [18,19] suggested that the transverse crack formation in the off-angle plies in a laminate of a particular stacking sequence would eventually reach an equilibrium state, beyond which no new cracks would form. The equilibrium crack spacing, associated with this characteristic damage state, could be achieved regardless of the loading history of the specimen. Hence, for laminates of the same stacking sequence, a specimen cycled at high stresses for a few cycles and one cycled at low stresses for many cycles, would develop at the characteristic damage state before fracture would occur.

The pattern of the transverse cracks that form in the off-axis plies in a laminate is controlled by the through-the-thickness constraint effects imposed by the neighbouring plies, and is not influenced by the presence of an embedded flaw. An analytical model, which uses an equilibrium element approach, has been adapted to examine the characteristic spacing of the transverse cracks in the off angle plies in these laminates [26]. The assumptions and postulations of the model will be briefly discussed below. Figure 28 shows a schematic of the idealized damage situation. The diagram represents an edge view of a transverse crack of width, a, in the middle 90° plies of a laminate. The neighboring plies on either side of the cracked ply have an orientation of α degrees to the loading axis. The disturbance caused by the broken layer is assumed not to extend beyond the first constraining (unbroken) ply on either side of the broken ply. Furthermore, any gradients in response from ply to ply are estimated to occur over a distance, b, which extends for a distance of one twentieth of the ply width into each ply. It is postulated that the cracks are spaced apart by the distance required for the stress in the broken layer to return to the value in the unbroken part of the layer away from the crack. The postulation is based on the idea that at the saturation spacing load level, there will be a crack each place the stress reaches the uncracked level in the ply being considered. Hence, as one moves away from a crack surface, the constraining adjacent plies transfer stress back into the cracked ply until, at a distance equal to the saturation spacing, the stress reaches the undisturbed value in the ply and is sufficient to form another crack at that location. The implication is that the stress

has reached a level which is sufficient to crack all material elements in a given ply or plies; but each time a crack forms, it relaxes the (axial) stress for a characteristic distance, depending on the stacking sequence of the laminate, on either side of the crack producing the equilibrium spacing observed. The analytical prediction of crack spacings was compared with experimental observations and there was good agreement between the equilibrium spacing predicted and the average crack spacing obtained from edge replicas of laminates of several stacking sequences. In the case of a $[0/90]_s$ laminate, the predicted value of the crack spacing of the transverse cracks in the 90° plies was slightly higher than that obtained for the type 3 specimens.

In the case of the type 5 $[\pm 45/90]_s$ flawed laminates, the pattern of the formation of the transverse cracks in the middle 90° plies was still governed by the through-the-thickness constraint effect imposed by the adjacent ±45° plies. Here, a different kind of constraint effect was also present, introducing an additional damage mode. Because of the stacking sequence of the laminate, tensile interlaminar normal stress existed at the free edges of the specimen causing delamination of the 90° plies and between the -45/90 and +45/-45 interfaces when the laminate was stressed. The delamination damage mode dominated the static and fatigue response of the material, and fracture generally occurred when the delamination had propagated across the half-width of the specimen before the regular spacing of the transverse cracks in the 90° plies could be achieved.

When the embedded transverse flaw was placed in a 0° ply, the situation became more complex because of the complex stress state near

the embedded flaw region. The region became the originating place of damage and damage development, and had a direct influence on the static and fatigue behaviour of the type 4 and 6 laminates. In the unconstrained situation (type 1 specimens), the major damage mechanism was axial splitting at the notch tips, and failure was generally associated with complete separation along the crack plane with very little breakage of the 0° fibers. The failure mode was longitudinal and hence the 0° fibers were not efficiently carrying the applied load. The damage mode was effectively suppressed when the embedded flaw was constrained by ±45° plies (Figure 7), such as in the type 6 specimens. The static failure of these laminates involved a transverse fracture of the 0° plies originating from the notch tips, indicating that some stress concentration effect due to the embedded flaw was present. When 90° plies were used to constrain the embedded flaw growth in the flawed 0° ply (type 4 specimens), the axial cracking at the notch tips in the interior 0° ply was only partially suppressed. However, there were other axial cracks developing away from the notch location in the 0° plies, and the 0° plies failed in a transverse mode.

The principal contributors to notched strength and changes in notched strength in a flawed ply under quasi-static loading is the in-plane constraint effects imposed on the notched ply by the constraining adjacent plies. An understanding of the in-plane constraint effect can be achieved by looking into the Poisson's effect which causes the transverse dimension of a specimen to change in proportion to the longitudinal extension experienced whenever a coupon of any material is stretched or loaded. In the case of a unidirectional composite lamina, Poisson's

ratio is directly related to the orientation of the fibers with respect to the loading direction. Poisson's ratios for 0° and 90° graphite/epoxy laminates were approximately 0.3 and 0.03 respectively, and Poisson's ratio for a ±45° laminate was estimated to be about 0.78 (from literature). Hence, when a laminate consisting of 0 and 90 degree plies, or 0 and ±45 degree plies, or any combination of ply orientations is subjected to tensile loading, the transverse dimension of each individual ply will attempt to contract to a dimension that the Poisson ratio of the ply dictates. Because of the bonding of plies together to form a laminate, it is seldom that any individual ply is able to achieve the dimension that it would achieve in the unconstrained situation. A common transverse dimension is then imposed on all the plies in the laminate, resulting in transverse stresses (σ_y) that exist in each ply which can be either tensile or compressive depending on values of Poisson's ratios of the ply and its adjacent plies.

An approximate value of the transverse stress (σ_y) can be estimated using values of Poisson's ratios of the plies involved. To apply the scheme one first calculates a "differential Poisson's ratio" defined as the absolute difference between the Poisson's ratio of the ply in question when that ply is unconstrained and the laminate Poisson's ratio when the subject ply is bonded into the laminate of interest. Analytically the expression is stated as

$$\Delta\nu = |\ \nu\ \text{(constrained)} - \nu\ \text{(unconstrained)}| \qquad (13)$$

For any given axial loading, represented by an axial strain of ε_x°, the "constraint effect" in the transverse direction is then given by

$$\Delta\nu\varepsilon_x^\circ \qquad (14)$$

The transverse normal stress in the subject ply is then approximated by

$$\sigma_y^i = E_y^i \, \Delta\nu\varepsilon_x^\circ \tag{15}$$

where E_y^i is the engineering Young's modulus of the subject ply in the transverse (y) direction.

Using the above approximation method, the results obtained for σ_y stresses were found to agree well with values calculated from a standard laminated plate analysis. For a 0° ply constrained on both sides by 90° plies, the σ_y constraint stress was positive (tensile), whereas when the constraining plies were ±45° plies, the transverse stress acting on the 0° ply was negative (compressive). In both cases, the stress σ_y was significant in magnitude - enough to influence the response of the laminate itself. Hence, there should be a greater tendency for axial splits to occur in the interior 0° plies of the $[90/0]_s$ laminate because of the tensile transverse stress present. By the same logic, the negative σ_y stress in the 0° plies of a $[\pm45/0]_s$ laminate should suppress such cracks from forming.

The situation is more complex when a notch is present. There are generally two basic modes of degradation at a notch in a unidirectional orthotropic lamina: a shearing mode where a plug of material pulls out above and below the open crack surfaces by a shearing motion (Fig. 29a), and a crack opening mode whereby normal stresses develop across planes perpendicular to the crack and the crack plane (Fig. 29b). The resistance to shear for a $[\pm45/0]_s$ laminate is nearly five times as great as the $[90/0]_s$ laminate due to the orientation of the ±45° plies, and the presence of a compressive transverse stress (σ_y) in the 0° plies of a

$[\pm 45/0]_s$ laminate helps to reduce the effect of the crack opening damage mode. Because of this, the fracture modes of the 0° plies in the types 4 and 6 specimens under static loading were significantly different (Figure 7), with a more severe case of axial splitting in the $[90/0]_s$ flawed laminates.

It is also interesting to note that minimum damage in a laminate does not necessarily correspond to maximum strength. To compare strengths, the net section stress in the 0° plies was calculated using the static tensile strength data from Table 2 and applying a laminated plate analysis. The strength of the unnotched unidirectional 0° lamina was about 147 Ksi. When a transverse center notch was added, the strength dropped to 73 Ksi. For the embedded flawed specimens, the net section stresses in the interior 0° plies were 177 Ksi in the case of 90° constraining plies (type 4 specimen) and 145 Ksi in the case of ±45° constraining plies (type 6 specimen). The presence of constraint effects helped to suppress the axial splitting damage mode in the notched 0° plies and distributed the applied load more effectively to the 0° fibers, resulting in a higher net section strength. Some retention of the stress concentration effect due to the embedded notch was shown in the $[\pm 45/0]_s$ laminate from the fracture mode of the 0° ply and the lower net section strength obtained.

In the fatigue testing of the types 4 and 6 specimens, it was found that two major fatigue damage modes were present: axial splitting at the notch tips in the interior 0° plies and delamination at the ply interfaces. The damage pattern of the $[90/0]_s$ flawed laminate was an "H" shaped pattern while that for the $[\pm 45/0]_s$ laminate showed no

indication of preferred damage growth. In both cases, the extent of fatigue damage in these specimens increased with increasing cycles of fatigue and increasing maximum cyclic stress. Again, the nominal stress in the interior 0° plies of the laminates was used as a common parameter in order to evaluate the effects of different orientations of the constraining plies on the damage development in the materials.

Some of the effects of the orientation of the constraining plies can be seen in Figs. 30 and 31. Figure 30 compares the c-scans of a type 4 $[90/0]_s$ laminate with a type 6 $[\pm 45/0]_s$ laminate after 100k cycles. The applied maximum stress was such that the nominal maximum stress in the 0° plies was 70 percent of the tensile strength of 0° unidirectional laminates with a center notch (type 1 specimens). The damage zone in the $[90/0]_s$ specimen had the "H" shape mentioned previously with damage extending away from the notch tips in the 0° direction. This c-scan also showed defective areas throughout the $[90/0]_s$ specimen whereas the defective region was confined to the flaw area in the $[\pm 45/0]_s$ specimen. Visual observation of the $[90/0]_s$ specimen showed that these defects were delaminations of the 90/0 interface which allowed the exterior 90° ply to peel off. At applied stresses such that the 0° ply stress was equal to the notched tensile strength of unidirectional specimens, the damage zone in the $[90/0]_s$ specimen was much larger than in the $[\pm 45/0]_s$ specimen after the same number of cycles (Fig. 31). The "H" pattern had extended toward the grip region; however, the damage zone in the $[\pm 45/0]_s$ specimen was again confined to the embedded flaw region.

The effect of the orientation of the constraining plies on the

damage growth can also be reflected by a comparison of the stiffness changes in these specimens (Fig. 32). The two specimens with nominal 0° ply stresses equal to 70 percent of the notched unidirectional tensile strength (type 4, 36 percent UTS and type 6, 41 percent UTS) suffered the same percent degradation of stiffness during the first 300k cycles, after which the stiffness of the $[\pm 45/0]_s$ specimen remained constant and the stiffness of the $[90/0]_s$ specimen continued to decrease. At nominal 0° ply stresses equal to the notched strength of unidirectional notched specimens (type 1) the percent stiffness change was greater in the type 4 (51% UTS) specimen than in the type 6 specimen (63% UTS). Again, the stiffness of the $[\pm 45/0]_s$ specimen initially decreased and remained constant whereas the stiffness of the $[90/0]_s$ specimen continued to decrease for 100k cycles. AT 70 percent UTS, the damage in the $[90/0]_s$ specimen had extended to the grips by 100k cycles with a corresponding stiffness decrease of 70 percent. As the damage continued to spread across the width of the specimen the stiffness also continued to decrease.

The fatigue damage of laminates with notched interior 0° plies is greatly influenced by the constraint effects imposed on the flawed ply by its adjacent neighbouring plies. Here, judging from the fatigue damage modes discussed, both the in-plane and the through-the-thickness constraint effects were acting to control the damage growth in the material. Transverse σ_y stresses were present in the plane of the lamina in the 0° ply as a result of the differential Poisson effect that existed between the plies. In the presence of the embedded transverse flaw, the σ_y stresses produced an in-plane constraint effect which could

either promote or suppress the formation of axial splits at the notch roots in the 0° ply depending on the magnitude and sign of the stresses.

Because the 0° plies are the principal load-carrying members in the laminates discussed, it is much more difficult to analyze the through-the-thickness constraint effects that also affect the fatigue damage development in these specimens. The stress state around the embedded flaw is extremely complex and the flaw itself is the origin of damage and damage growth in the laminates. A three-dimensional finite difference scheme developed by Talug [27] has been used to calculate and to analyze the stress field in the neighborhood of the interior crack in a laminate. Stress distributions of two stresses that exist at the embedded flaw region which may influence the damage development of the types 4 and 6 specimens are shown in Figs. 33-35. In all cases, the stresses were calculated using the finite difference scheme with an applied strain value of $\varepsilon_x = 10^{-3}$ in/in and $\varepsilon_y = -2 \times 10^{-4}$ in/in.

Figure 33 shows the through-the-thickness normal stress, σ_z which develops at the interface between the broken and unbroken plies. This out-of-plane stress is a stress component which promotes the delamination mode of damage in these laminates. The stress levels were significant and were greatest in the $[90/0]_s$ case. A through-the-thickness shear stress, τ_{xz}, also existed at the embedded notch and is plotted in Figs. 34 and 35 for the types 4 and 6 specimens respectively. The distribution of the shear stress for the two laminates is quite similar suggesting that the 0° plies control the distribution. The magnitude of the stresses was again significant enough to participate in the damage growth. Furthermore, it can be shown that axial stress elevation due to

the notch in a constrained notched ply situation is highest when the constraint layer has the lowest modulus or strength.

All the factors described above contribute to the state of stress in the flawed 0° ply laminates and govern the damage development in the laminates while under fatigue loading. The combined effect of the in-plane and through-the-thickness constraints on the flawed 0° ply predicts a less severe damage situation for the ±45° constraining case when compared to the 90° constraining case which consists of a greater degree of axial splitting and delamination. The prediction agrees well with the experimental results obtained for the types 4 and 6 specimens tested.

From the designer's viewpoint, one important possible consequence of the investigation of constraint effects is the development of sufficient understanding to enable one to construct design criteria through which one can optimize parameters such as strength, stiffness, fatigue life, and residual strength. The results obtained, thus far, indicated that, in the design of composite structures, a compromise has to be reached with regard to maximizing the desired properties of the material. Both the static and fatigue results of the flawed 0° ply laminates have shown that maximum constraint on the flawed ply does not produce minimum damage in the laminate. Also, the lesser degree of damage (in terms of the axial splitting and delamination), in the biaxially constrained flawed laminates did not result in a higher residual laminate strength or longer fatigue life.

At high cyclic stress levels (with the nominal stress in the interior 0° ply equal to 130 percent of the notched tensile strength of type 1 specimens), although the $[90/0]_s$ flawed laminate exhibited a large

degree of delamination and the axial splits at the notch tips of the flawed 0° ply had propagated up into the gripped region, the specimen survived a million cycles of testing and appeared to be in a fairly stable condition. At the same nominal cyclic stresses in the 0° plies, the $[\pm 45/0]_s$ flawed laminates failed within the first 10,000 cycles although the fatigue damage in the specimen was less severe and was localized within the flawed region. Hence, the crossply constraint is more desirable in the case of the flawed 0° ply laminates from the standpoint of strength and fatigue life.

If a stiffness based design criteria is used, a completely different set of conclusions is reached based on the available data. For the same nominal cyclic stress in the 0° plies, the degradation in the laminate stiffness was considerably less in the biaxially constrained case than the crossply constraint situation. Hence, in the design of composites, there is a trade-off existing between optimizing strength, stiffness, residual strength and fatigue life. In maximizing one parameter, one might have to sacrifice other requirements on the other material properties in the design.

V. CONCLUSIONS

An investigation was conducted to study the constraint effects on flaw growth in composite laminates. Results presented were for the case when a transverse flaw was placed in an interior ply perpendicular to the loading axis. Two orientations of the flawed ply were examined (0 and 90 degrees), and two distinctly different constraint cases were studied (cross-ply constraint and biaxial constraint).

The approach used consisted of evaluating constraint effects as they influenced the behaviour of the flawed plies. The response of the unconstrained notched situation was first determined and the effect of adding on various angle plies to the flawed lamina was then treated as the "constraint effect."

Throughout the study, various nondestructive testing methods were employed to evaluate the material response and to determine the damage and damage growth in the specimens. Although some NDE methods were more capable of detecting certain particular types of defects, the use of a combination of certain NDE methods during the testing proved to be an effective way of determining the damage state in the material.

The presence of the embedded notch had no significant influence on the behaviour of the flawed 90° ply specimens, although in some cases certain inherent unintentional defects proved to be critical in nature. The through-the-thickness constraint effects from the adjacent plies control the pattern of formation of the transverse cracks in the off-axis plies, giving rise to a characteristic damage state in the laminate, which is characteristic of a particular stacking sequence of the laminate and is independent of the loading history of the specimen.

Interlaminar normal stress at the free edge of the $[\pm 45/90]_s$ flawed laminates caused delamination of the 90° plies and -45/90 interfaces which became the dominating damage mode in the specimens tested.

In the flawed 0° ply laminates, the embedded transverse flaw in the 0° ply was the origin of damage and damage development in the laminates. The static response of such specimens was controlled mainly by the in-plane constraints which governed the damage modes in the 0° ply and influenced the fracture behaviour of the laminates, contributing to the notched strength and changes in notched strength of the material. In general, maximum constraint on the flawed ply does not necessarily correspond to minimum damage, and minimum damage does not give rise to maximum strength. The axial splitting of the 0° ply at the notch tips was more effectively suppressed by the biaxial constraint, but the $[\pm 45/0]_s$ flawed specimens also showed a greater notch stress concentration effect when pulled to failure, i.e., a comparatively lower strength.

Two major damage modes were present in the fatigue damage development of the flawed 0° ply specimens: axial splitting of the 0° ply at the interior notch roots and delamination of the ply interfaces. In the $[90/0]_s$ specimens, transverse cracks first occurred in the outer 90° plies, relaxing the constraint on the flawed 0° ply. The axial splits developing at the notch roots in the 0° ply then caused delamination of the 90/0 interfaces along the split lines due to the shearing motion between the outer ligaments of the 0° ply and the inner strip of material above and below the notch which developed between the two axial splits. The fatigue damage in the $[\pm 45/0]_s$ flawed specimens was more localized, with delamination of the +45/-45 and -45/0 interfaces at the

flawed region. Axial splits that developed in the interior 0° ply of the $[\pm 45/0]_s$ specimens were confined to a relatively small delaminated zone.

The nominal axial stress in the interior 0° plies was selected as the common loading parameter in evaluating the effects of the orientation of the constraining plies on the interior flaw growth in these laminates. For the same nominal 0° ply stress, the damage and damage development of the $[90/0]_s$ specimens was considerably more severe than that of the $[\pm 45/0]_s$ specimens. The presence of the interior flaw produced out-of-plane normal stress (σ_z) and shear stress (τ_{xz}) at the flaw because of the through-the-thickness constraint imposed. The magnitude of these stresses was significant and could promote delamination of the ply interfaces at the flaw location.

The residual strengths and residual failure modes of the flawed $[90/0]_s$ and $[\pm 45/0]_s$ fatigue specimens were dependent on the type and extent of fatigue damage present. A minimum amount of fatigue damage did not necessarily give the longest fatigue life or the highest residual strength.

Finally, the damage modes and the extent of damage in composite laminates with an internal flaw and subsequent changes in the material properties are governed by the internal stress state as determined by the constraining plies and the relationship of the stress state to the strength state. In the design of composites, a compromise has to be reached with regard to optimizing strength, stiffness, residual strength and fatigue life. In maximizing one parameter, one might have to sacrifice other requirements on the other material properties in the

design.

The present investigation has identified the important constraint parameters, investigated their origin and their importance, and established a philosophy of constraint effects which can be used, in general, to calculate or estimate the influence of constraint on the notched response of composite laminates. This study was conducted on a particular notch configuration under a specific set of circumstances. Using the results obtained, and with further studies on other notch and constraint situations, a complete understanding of all aspects of constraint effects in composite laminates can be achieved.

REFERENCES

1. Stinchcomb, W. W. and Reifsnider, K. L., "Fatigue Damage Mechanisms in Composite Materials: A Review," presented at ASTM Symposium on Fatigue Mechanisms, Kansas City, Mo., May 1978.

2. Stinchcomb, W. W., Reifsnider, K. L., Williams, R. S. and Marcus, L. A., "Frequency Dependent Fatigue Damage Modes in Composite Materials," Failure Modes in Composites II, Met. Soc. AIME, 1975, pp. 3-15.

3. Mandell, J. F. and Meier, U. R. S., "Fatigue Crack Propagation in 0°/90° E-Glass/Epoxy Composites," Fatigue of Composite Materials ASTM STP 569, American Society for Testing and Materials, 1975, pp. 28-44.

4. Chang, F. H., Gordon, D. E., Rodini, B. T. and McDaniel, R. H., "Real-Time Characterization of Damage Growth in Graphite-Epoxy Laminates," J. Comp. Mat., Vol. 10, July 1976, pp. 182-192.

5. Porter, T. R., "Evaluation of Flawed Composite Structure Under Static and Cyclic Loading," Fatigue of Filamentary Composite Materials, ASTM STP 636, K. L. Reifsnider and K. N. Lauraitis, Eds., American Society for Testing and Materials, 1977, pp. 152-170.

6. Kendall, D. P., "Mechanisms of Fatigue Crack Growth in Boron/Aluminum Laminates," Fatigue of Filamentary Composite Materials, ASTM STP 636, K. L. Reifsnider and K. N. Lauraitis, Eds., American Society for Testing and Materials, 1977, pp. 47-56.

7. Chang, F. H., Gordon, D. E. and Gardner, A. H., "A Study of Fatigue Damage in Composites by Nondestructive Testing Techniques," Fatigue of Filamentary Composite Materials, ASTM STP 636, K. L. Reifsnider and K. N. Lauraitis, Eds., American Society for Testing and Materials, 1977, pp. 57-72.

8. Sendeckyj, G. P., Stalnaker, H. D. and Kleismit, R. A., "Effect of Temperature on Fatigue Response of Surface-Notched $[(0,\pm45,0)_s]_3$ Graphite-Epoxy Laminate," Fatigue of Filamentary Composite Materials, ASTM STP 636, K. L. Reifsnider and K. N. Lauraitis, Eds., American Society for Testing and Materials, 1977, pp. 123-140.

9. Ramani, S. V. and Williams, D. P., "Notched and Unnotched Fatigue Behavior of Angle-Ply Graphite Epoxy Composites," Fatigue of Filamentary Composite Materials, ASTM STP 636, K. L. Reifsnider and K. N. Lauraitis, Eds., American Society for Testing and Materials, 1977, pp. 27-46.

10. Roderick, G. L. and Whitcomb, J. D., "Fatigue Damage of Notched Boron/Epoxy Laminates Under Constant-Amplitude Loading," Fatigue of Filamentary Composite Materials, ASTM STP 636, K. L. Reifsnider and K. N. Lauraitis, Eds., American Society for Testing and Materials, 1977, pp. 73-88.

11. Reifsnider, K. L., Henneke, E. G. and Stinchcomb, W. W., "Delamination in Quasi-Isotropic Graphite Epoxy Laminates," Composite Materials: Testing and Design, Fourth Conference, ASTM STP 617, American Society for Testing and Materials, 1977, pp. 93-105.

12. Walter, R. W., Johnson, R. W., June, R. R. and McCarty, J. E., "Designing for Integrity in Long-life Composite Aircraft Structures," Fatigue of Filamentary Composite Materials, ASTM STP 636, K. L. Reifsnider and K. N. Lauraitis, Eds., American Society for Testing and Materials, 1977, pp. 228-247.

13. Underwood, J. H. and Kendall, D. P., "Fatigue Damage in Notched Glass-Epoxy Sheet," Proc. 1975 International Conference on Composite Materials, Met. Soc. AIME, 1976.

14. Smith, C. W., "Limitations of Fracture Mechanics as Applied to Composites," Inelastic Behaviour of Composite Materials, AMD, ASME, Vol. 13, 1975, pp. 157-175.

15. Henneke, E. G., II, and Duke, J. C., Jr., "A Review of the State-Of-The-Art of Nondestructive Evaluation of Advanced Composite Materials," Dept. of Engr. Sci. and Mechanics, VPI & SU, Blacksburg, Virginia, September 1979.

16. Liptai, R. G., "Acoustic Emission from Composite Materials," Composite Materials: Testing and Design (Second Conference), ASTM STP 497, American Society for Testing and Materials, 1972, pp. 285-298.

17. Williams, J. H., Jr. and Lee, S. S., "Acoustic Emission Monitoring of Fiber Composite Materials and Structures," J. of Composite Materials, Vol. 12, Oct. 1978, pp. 348-370.

18. Stinchcomb, W. W., Reifsnider, K. L., Yeung, P. C. and O'Brien, T. K., "Investigation and Characterization of Constraint Effects on Flaw Growth During Fatigue Loading of Composite Materials," Semi-Annual Status Reports I, II, III, Final Report, NASA Grant NSG-1364, Virginia Polytechnic Institute and State University, Dec. 1976-June 1979.

19. Reifsnider, K. L., Henneke, E. G., II and Stinchcomb, W. W., "Defect-Property Relationships in Composite Materials," AFML-TR-76-81, Part I, II, III, April 1976, 1977, 1978.

20. Stalnaker, D. O., "An Investigation of Edge Damage Development in Quasi-Isotropic Graphite-Epoxy Laminates," Thesis, Dept. of Engr. Sci. and Mech., Virginia Polytechnic Institute and State University, April 1976.

21. Hayford, D. T., Henneke, E. G., II and Stinchcomb, W. W., "The Correlation of Ultrasonic Attenuation and Shear Strength in Graphite-Polyimide Composites," J. of Composite Materials, Vol. 11, Oct. 1977.

22. Saluja, H. S., "Correlation of Damage and Ultrasonic Attenuation in Composites," Thesis, Dept. of Engr. Sci. and Mech., Virginia Polytechnic Institute and State University, Sept. 1977.

23. Reifsnider, K. L. and Williams, R. S., "Determination of Fatigue-Related Heat Emission in Composite Materials," Exp. Mech. 14, Dec. 1974, pp. 479-485.

24. Jones, R. M., Mechanics of Composite Materials, McGraw-Hill, 1975.

25. Gibbins, M. N., "Investigation of the Fatigue Response of Composite Laminates with Internal Flaws," Thesis, Dept. of Engr. Sci. and Mech., Virginia Polytechnic Institute and State University, Dec. 1979.

26. Reifsnider, K. L., "Some Fundamental Aspects of the Fatigue and Fracture Response of Composite Materials," Proc. 14th Annual Soc. of Engr. Sci. Meeting, Lehigh University, Nov. 14-16, 1977.

27. Talug, A., "Analysis of Stress Fields in Composite Laminates with Interior Cracks," Ph.D. Dissertation, Dept. of Engr. Sci and Mech., Virginia Polytechnic Institute and State University, August 1978.

TABLE 1--Graphite epoxy test specimens

Specimen Type	Orientation	Fiber Volume Fraction,%	Notch Configuration
1	$[0]_6$	65.6	Through slit perpendicular to fibers
2	$[90]_6$	64.7	Through slit parallel to fibers
3	$[0/90]_s$	63.6	Embedded slit in 90° plies parallel to fibers
4	$[90/0]_s$	61.7	Embedded slit in 0° plies perpendicular to fibers
5	$[\pm 45/90]_s$	65.0	Embedded slit in 90° plies parallel to fibers
6	$[\pm 45/0]_s$	63.8	Embedded slit in 0° plies perpendicular to fibers

TABLE 2--Average tensile strength of notched/flawed graphite epoxy specimens

Specimen Type	Orientation	Tensile Strength,Ksi
1	$[0]_6$	72.8 ± 11.8*
2	$[90]_6$	3.44 ± 0.30*
3	$[0/90]_s$	105.3 ± 9.64
4	$[90/0]_s$	82.0 ± 0.90
5	$[\pm 45/90]_s$	25.6
6	$[\pm 45/0]_s$	51.5

*Strength values calculated using net section areas at the notch for through-the-thickness notched specimens (1 Ksi = 6.895 MPa).

TABLE 3--Residual strength data for type 4 and 6 specimens

Specimen Type and Number	Load History (Cycles @ Stress)	Average Tensile Strength of Specimen Type (Ksi)	Residual Strength After Fatigue Loading (Ksi)	Net Section Stress in 0° Plies at Failure (Ksi)	
				Static (average)	Residual
4 $[90/0]_s$ #1	38K @ 120% σ_{NS}	82	72	164	156
* 4 $[90/0]_s$ #2	100K @ 100% σ_{NS}	82	82	164	163
* 4 $[90/0]_s$ #3	10^6 @ 100% σ_{NS}	82	85	164	168
* 4 $[90/0]_s$ #4	10^6 @ 130% σ_{NS}	82	91	164	172
6 $[\pm45/0]_s$ #1	10^6 @ 120% σ_{NS}	51	57	136	148
* 6 $[\pm45/0]_s$ #2	100K @ 100% σ_{NS}	51	46	136	120
* 6 $[\pm45/0]_s$ #3	10^6 @ 100% σ_{NS}	51	48	136	122

* New specimens

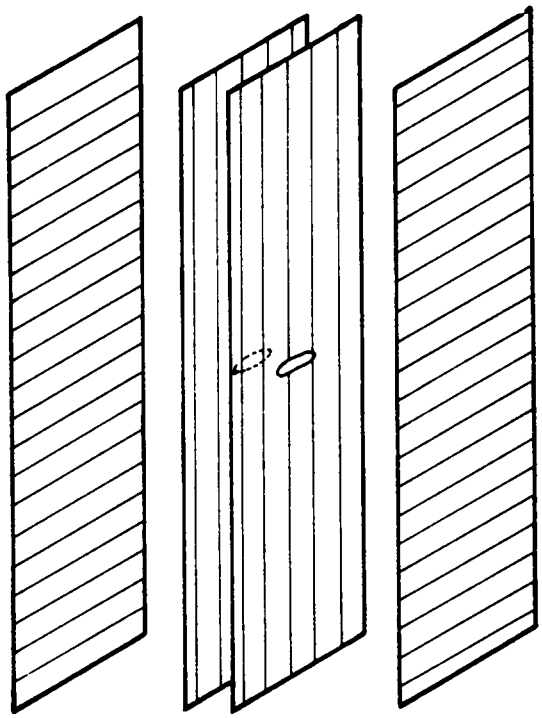

Fig. 1. A $[90/0]_s$ laminate with a transverse embedded flaw in the 0 degree plies.

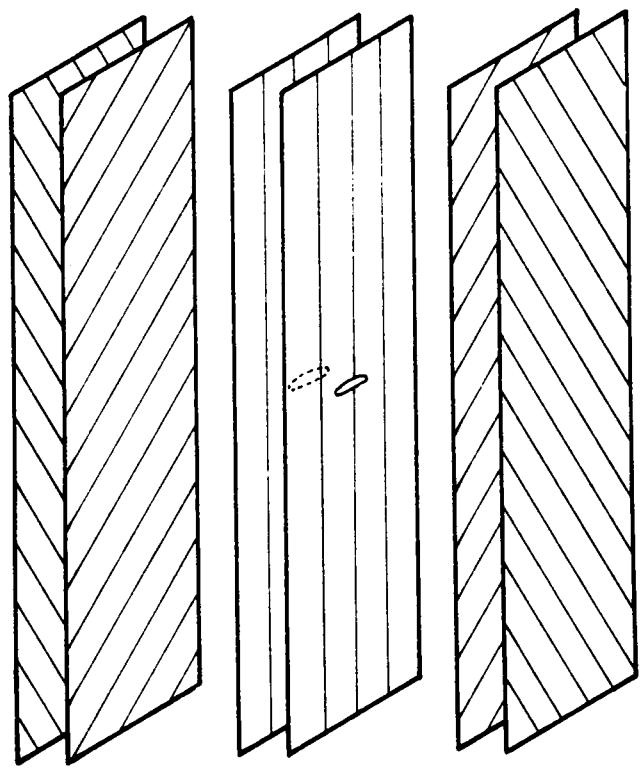

Fig. 2. A $[\pm 45/0]_s$ laminate with a transverse embedded flaw in the 0 degree plies.

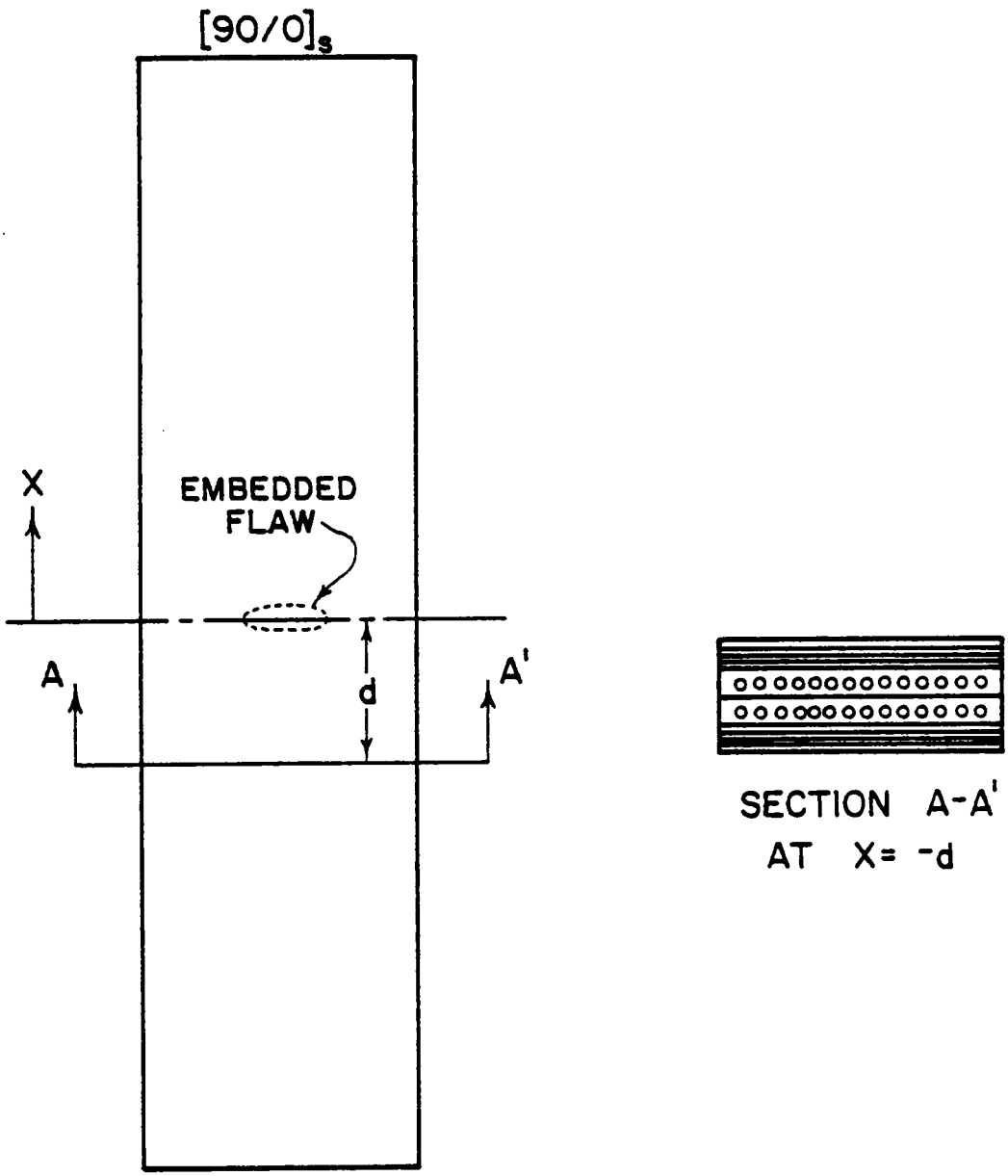

Fig. 3. Schematic diagram of sectioning studies on a typical $[90/0]_s$ type laminate with an embedded flaw in the interior 0 degree plies.

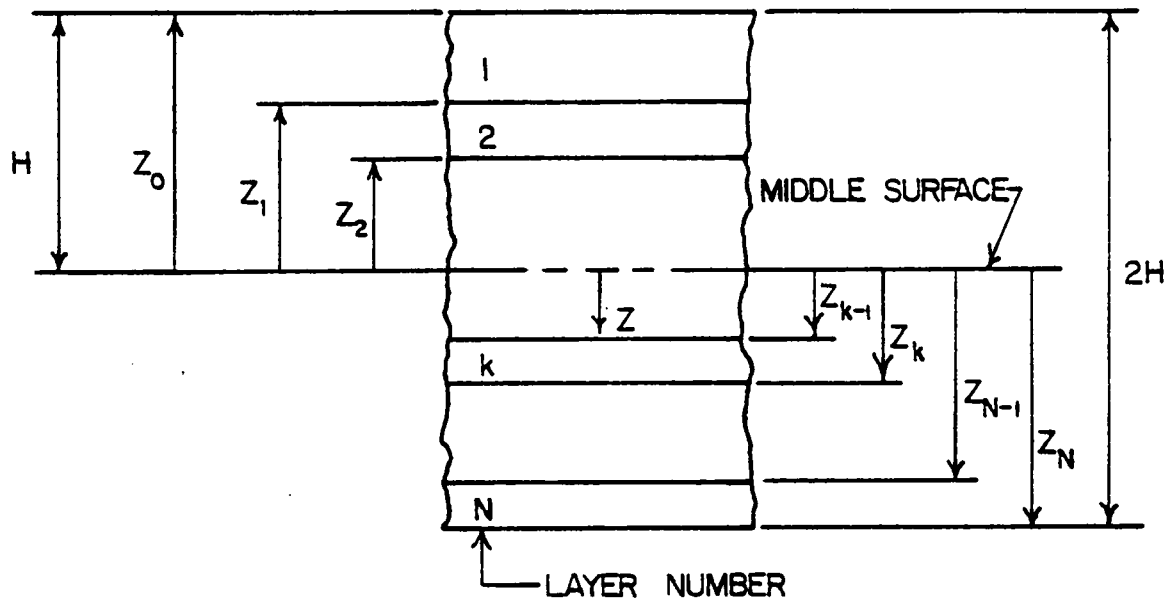

Fig. 4. Geometry of an n-layered laminate.

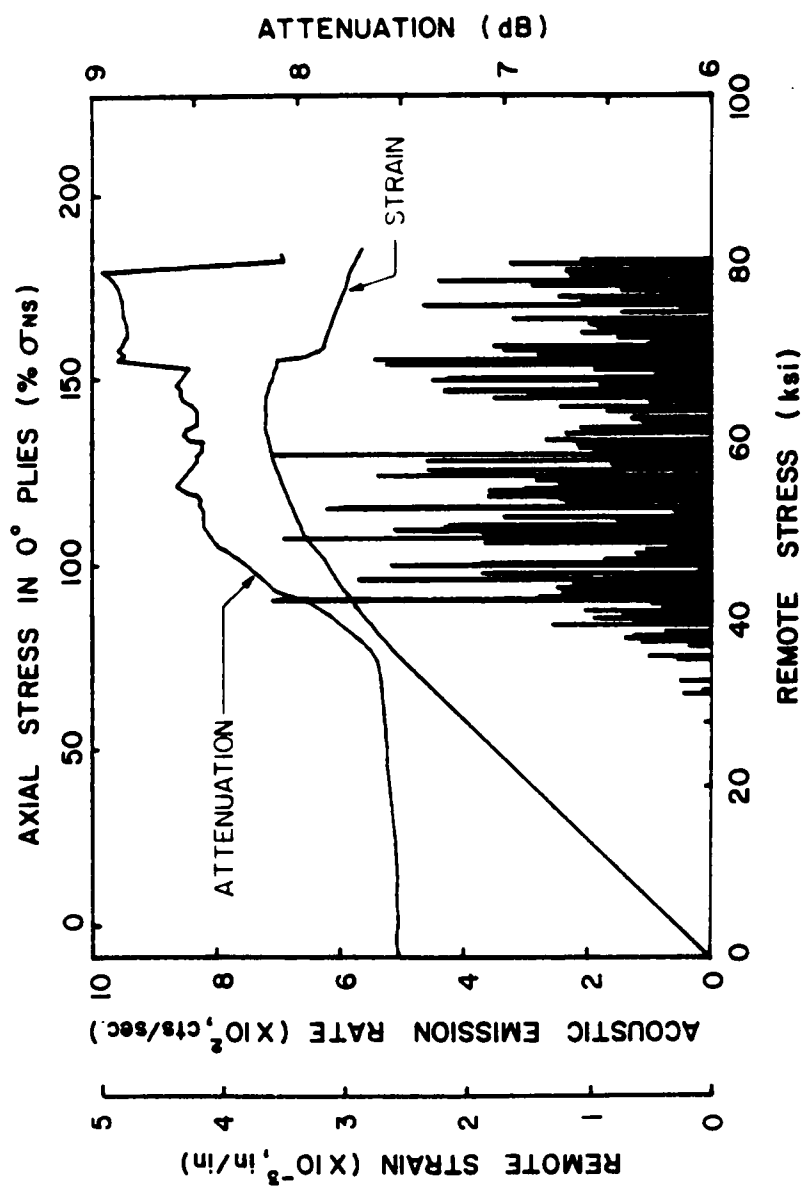

Fig. 5. Acoustic emission rate, ultrasonic attenuation, and remote strain vs. applied stress for a type 4 ($[90/0]_s$ with a transverse flaw in the interior 0 degree plies) specimen loaded statically to failure.

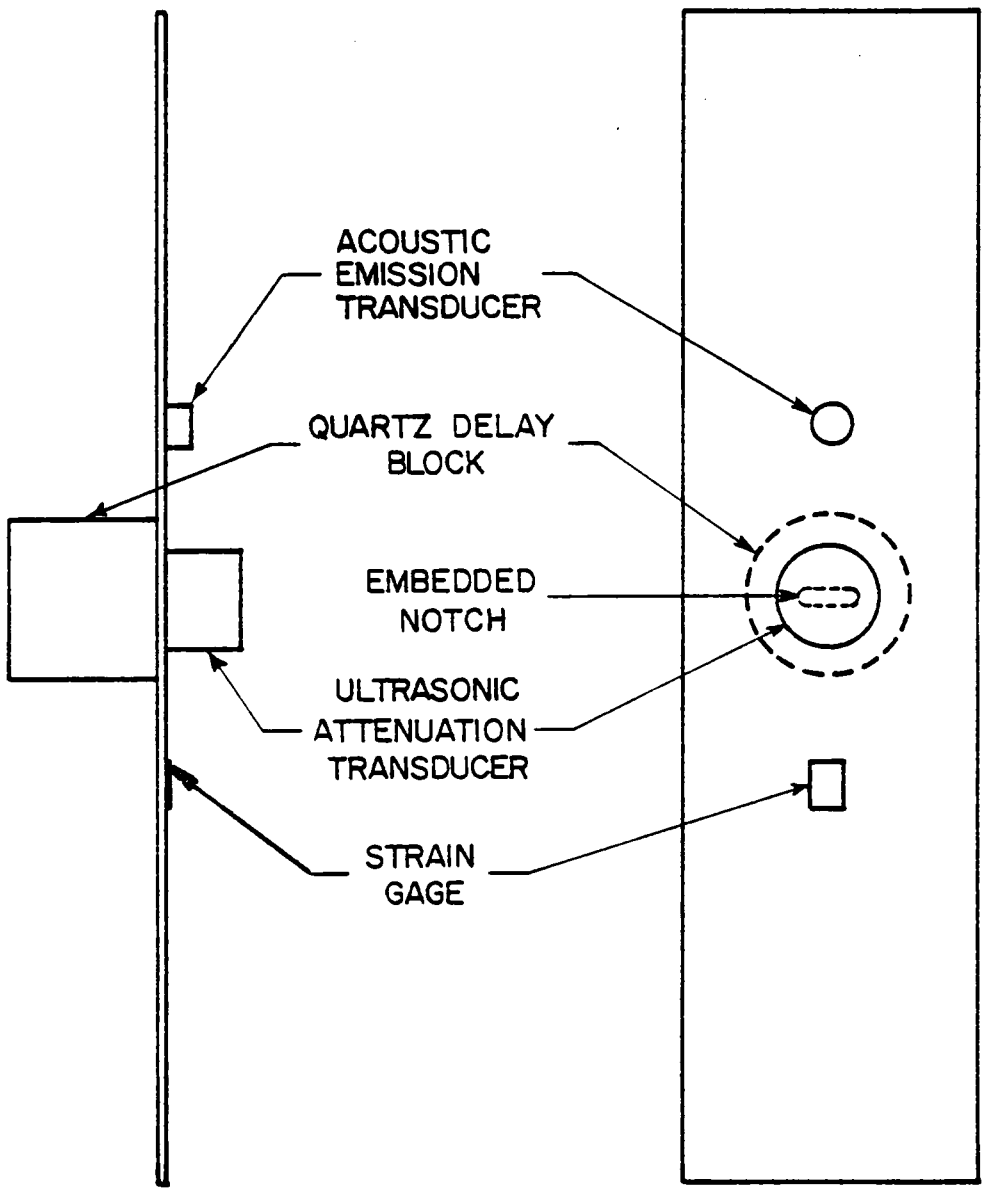

Fig. 6. Schematic diagram of apparatus set-up for static tension tests.

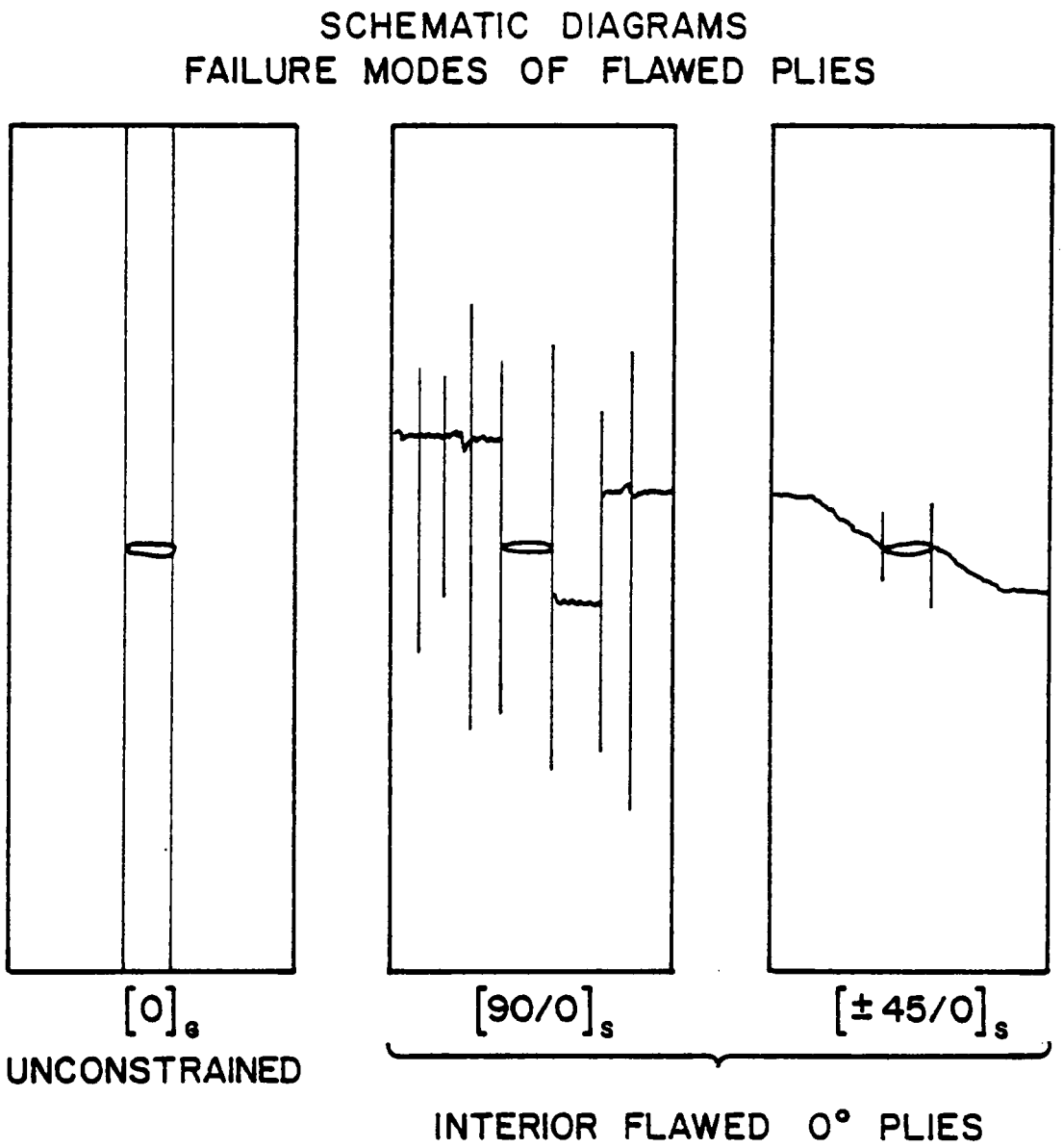

Fig. 7. Schematic diagram showing the failure modes of flawed 0 degree plies in the unconstrained and constrained situations.

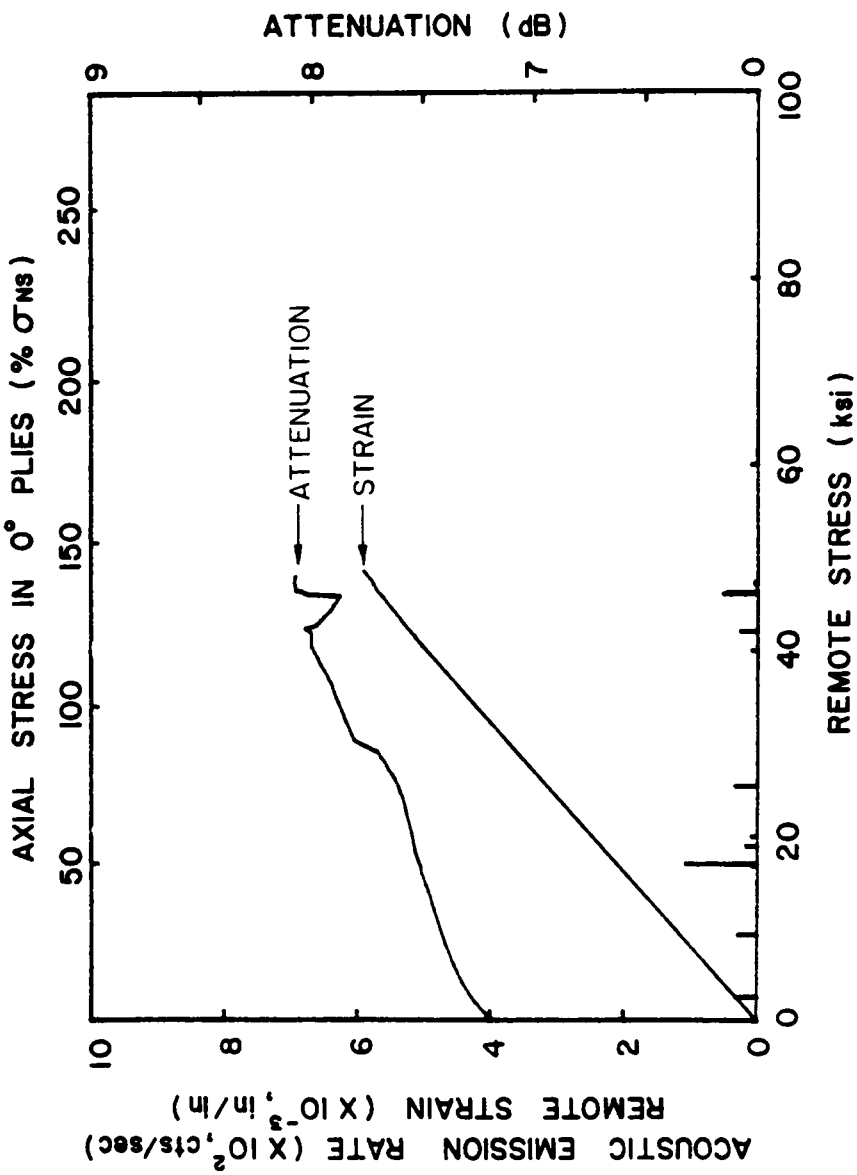

Fig. 8. Acoustic emission rate, ultrasonic attenuation, and remote strain vs. applied stress for a type 6 ($[\pm 45/0]_S$ with a transverse flaw in the interior 0 degree plies) specimen loaded statically to 2400 lbs.

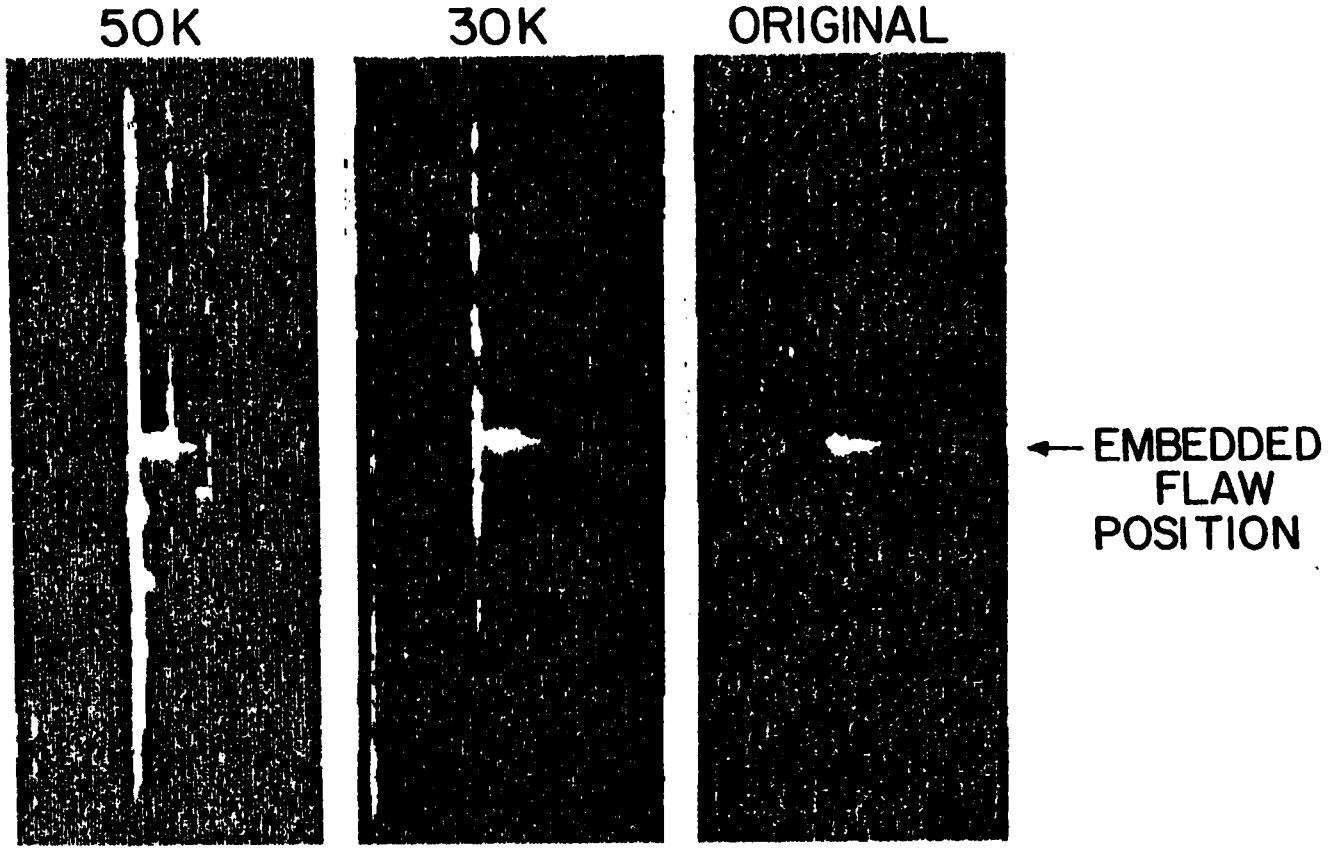

Fig. 9. Ultrasonic c-scan history of a type 3 $[0/90]_s$ flawed laminate under fatigue loading with a maximum cyclic stress equal to 80 percent of the ultimate tensile strength of the laminate.

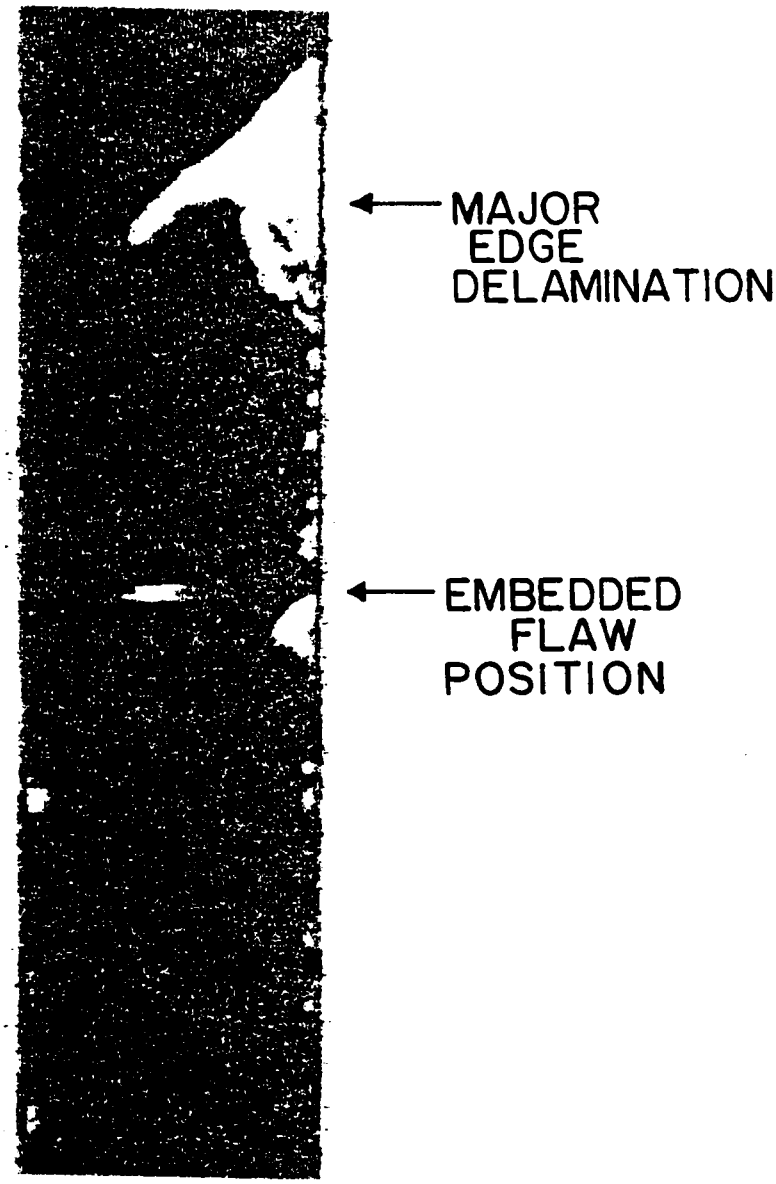

Fig. 10. Ultrasonic c-scan diagram of a type 5 $[\pm 45/90]_S$ flawed laminate after 88,000 cycles of fatigue loading with a maximum cyclic stress equal to 62 percent of the ultimate tensile strength of the laminate.

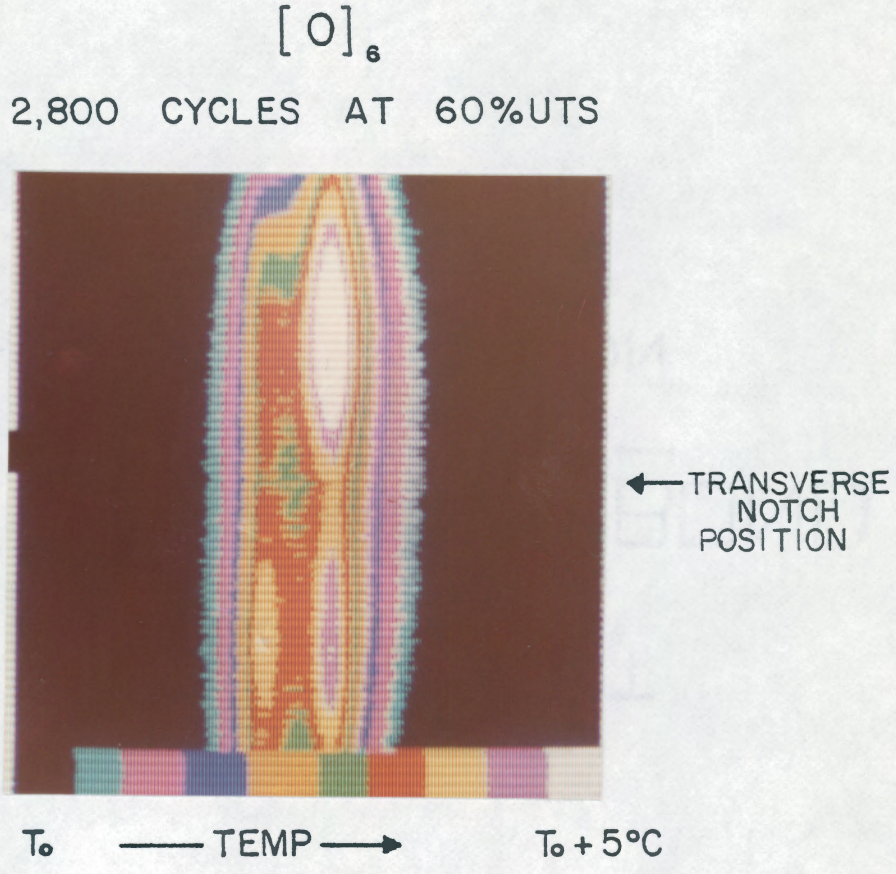

Fig. 11. Heat pattern of a type 1 $[0]_6$ laminate with a center transverse notch at 2,800 cycles of fatigue loading at 60% UTS.

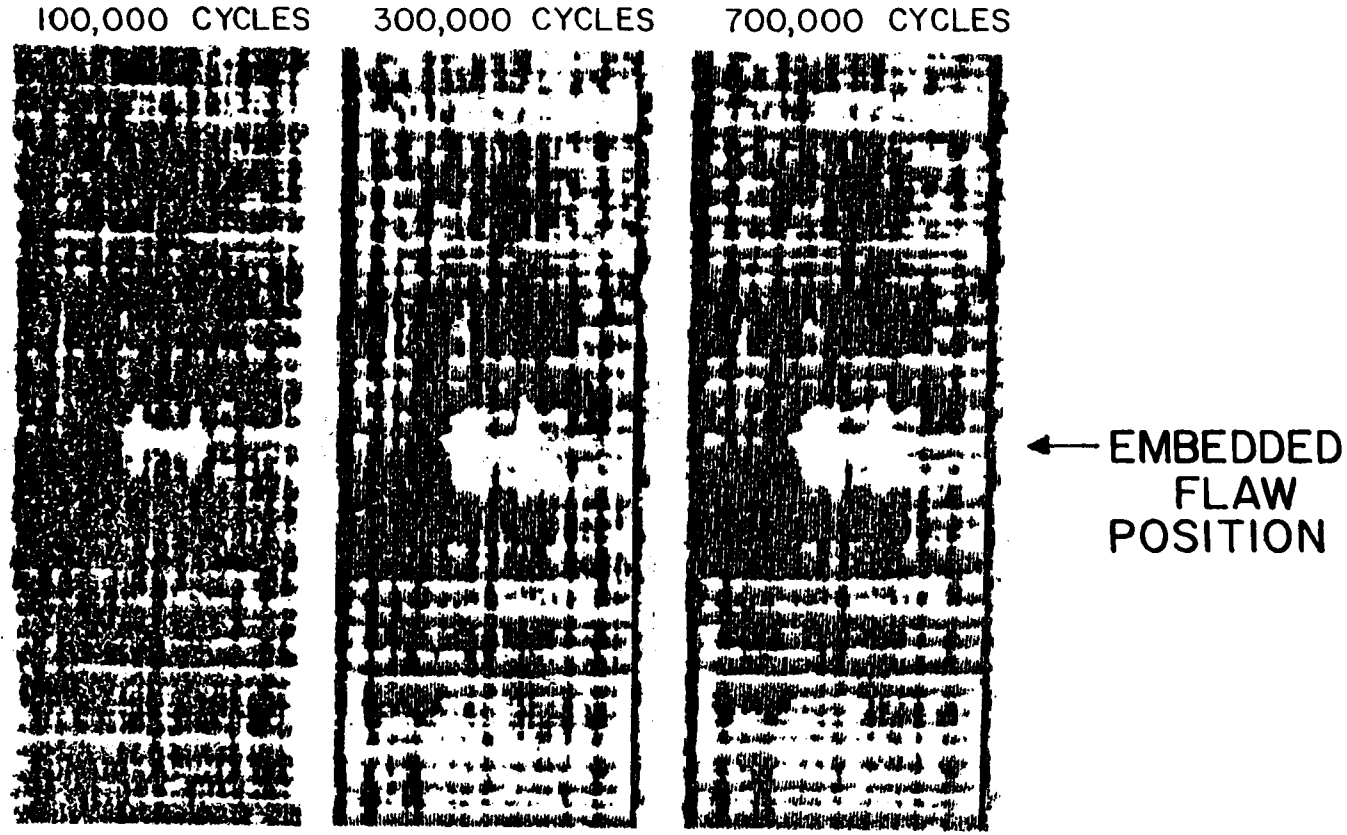

Fig. 12. Ultrasonic c-scan history of a type 4 $[90/0]_s$ flawed laminate under cyclic loading at 36% UTS. The nominal stress in the 0 degree plies is 70% of the notched tensile strength of the type 1 specimens.

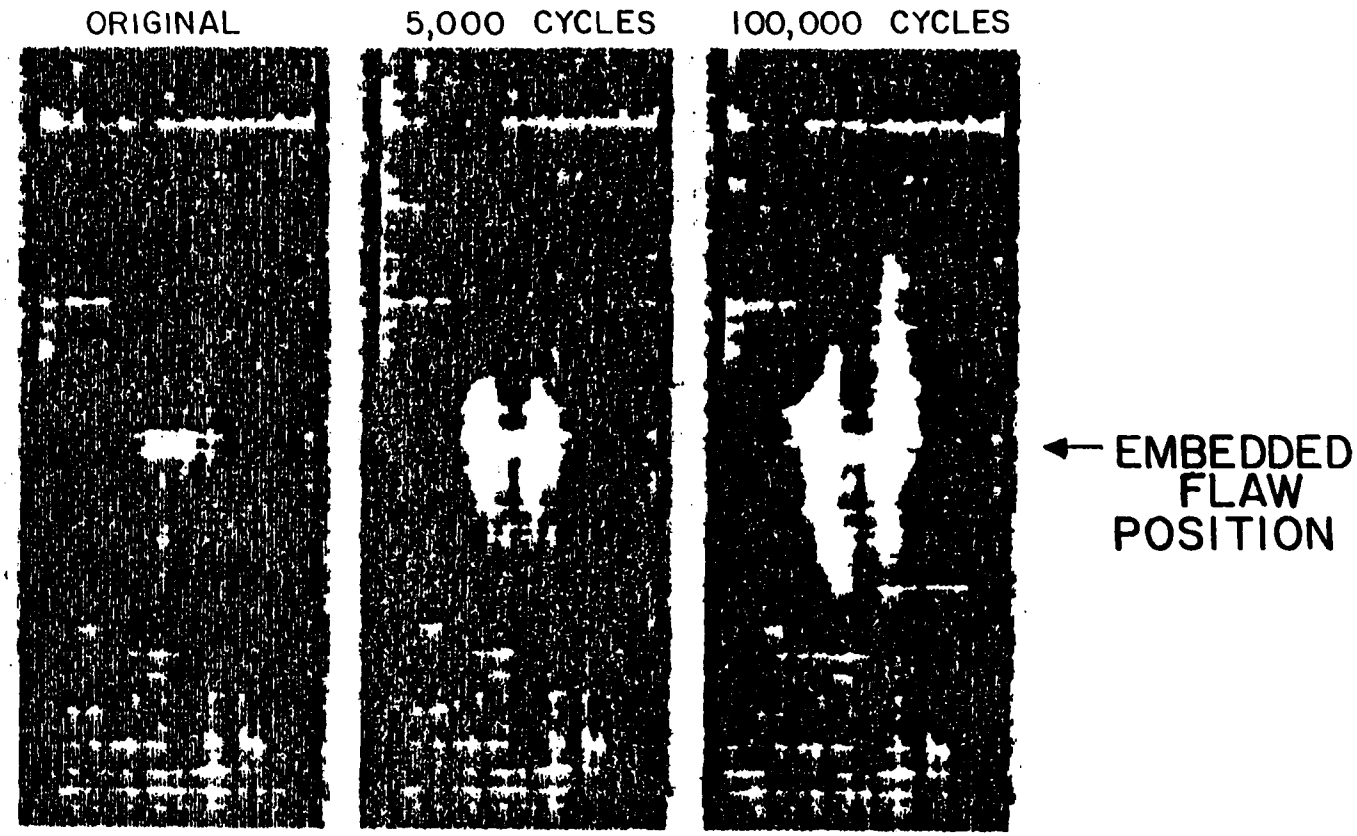

Fig. 13. Ultrasonic c-scan history of a type 4 $[90/0]_s$ flawed laminate under cyclic loading at 51% UTS. The nomimal stress in the 0 degree plies is 100% of the notched tensile strength of the type 1 specimens.

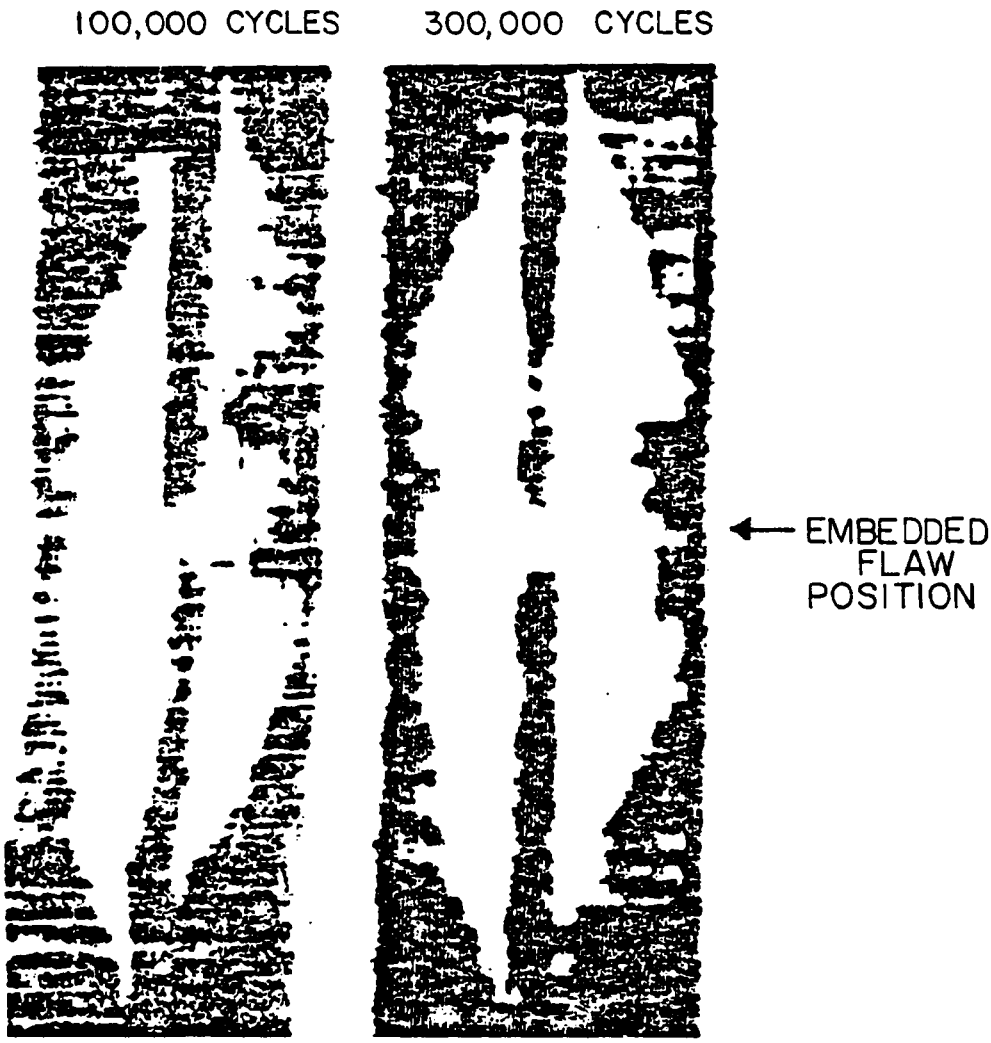

Fig. 14. Ultrasonic c-scan history of a type 4 $[90/0]_s$ flawed laminate under cyclic loading at 70% UTS. The nomimal stress in the 0 degree plies is 134% of the notched tensile strength of the type 1 specimens.

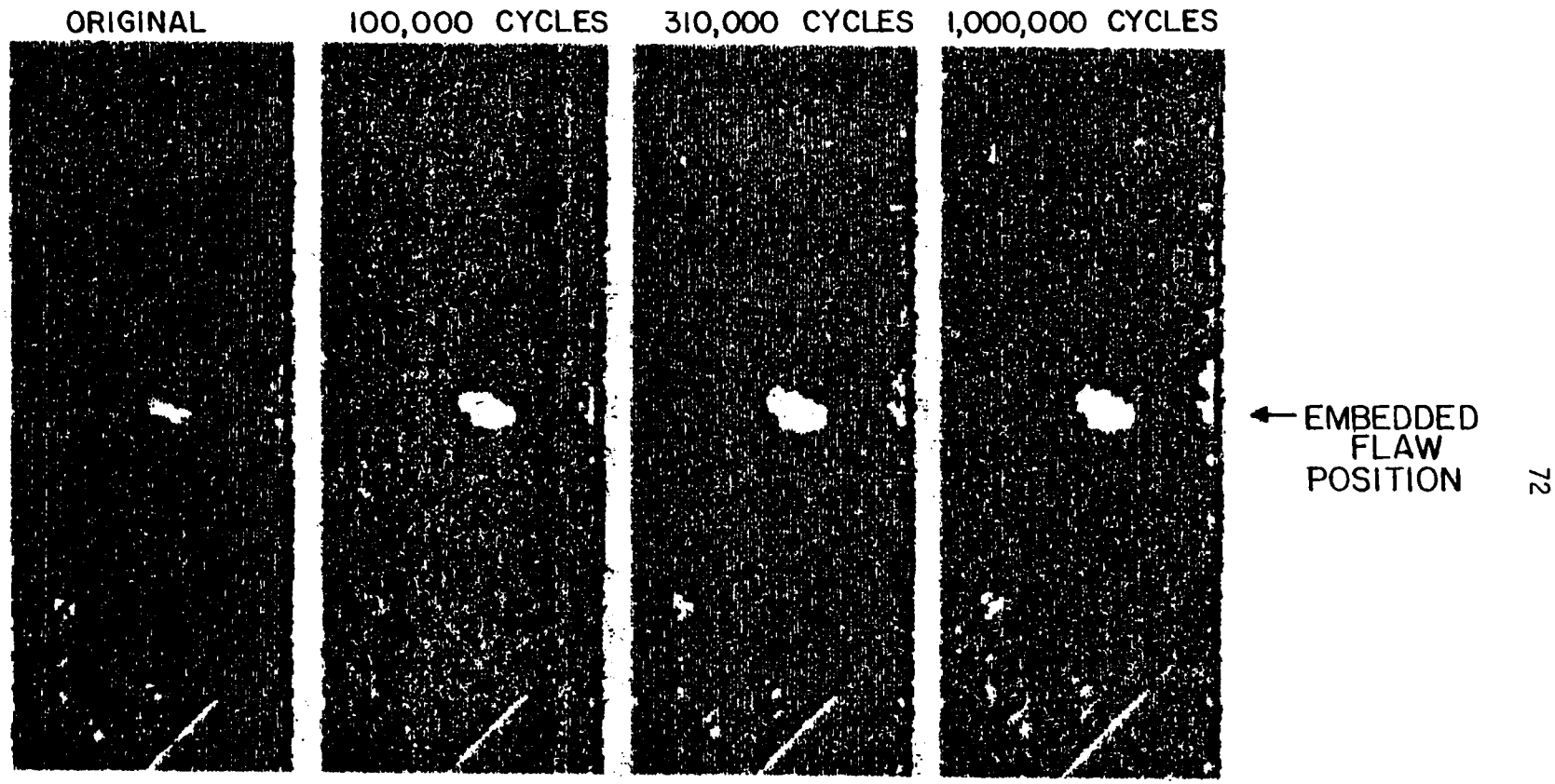

Fig. 15. Ultrasonic c-scan history of a type 6 $[\pm 45/0]_S$ flawed laminate under cyclic loading at 41% UTS. The nomimal stress in the 0 degree plies is 70% of the notched tensile strength of the type 1 specimens.

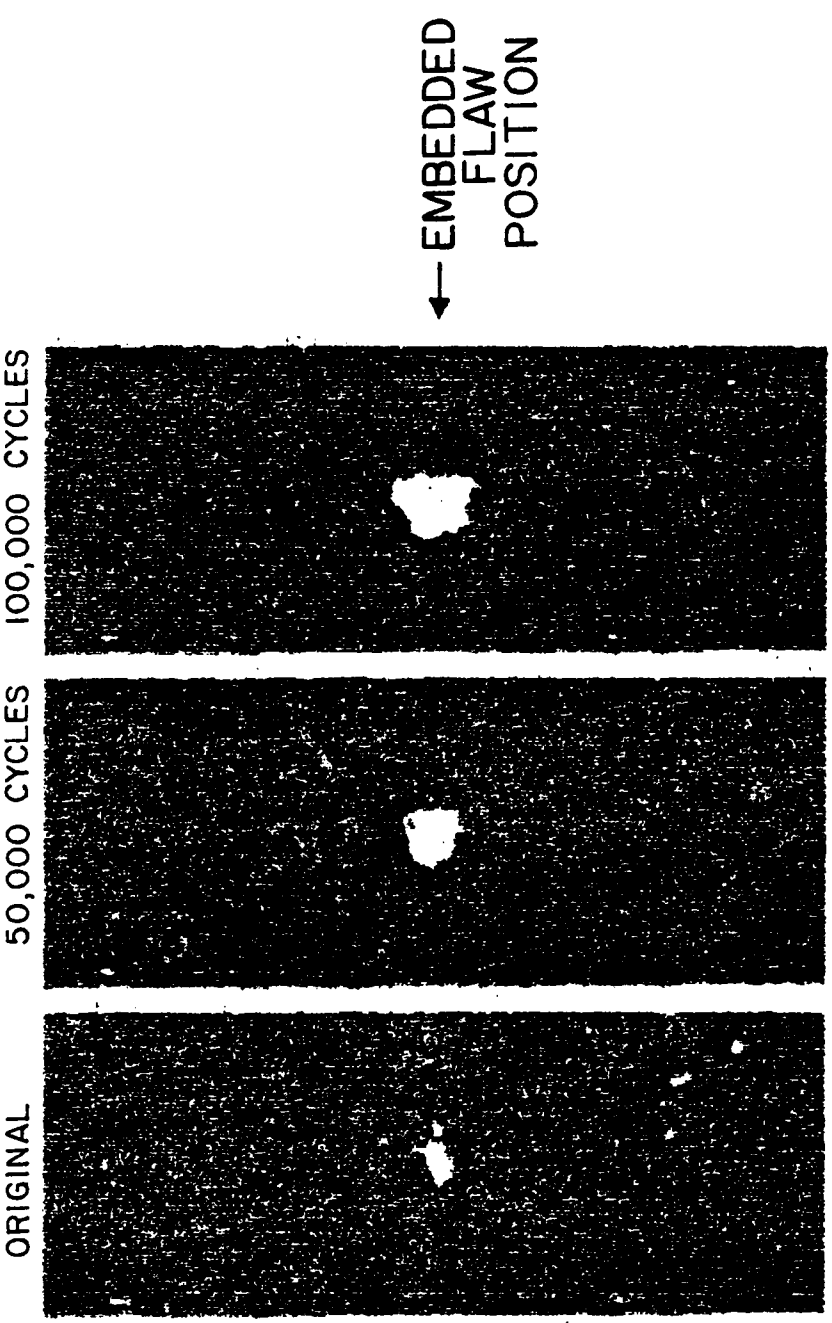

Fig. 16. Ultrasonic c-scan history of a type 6 $[\pm 45/0]_s$ flawed laminate under cyclic loading at 63% UTS. The nomimal stress in the 0 degree plies is 100% of the notched tensile strength of the type 1 specimens.

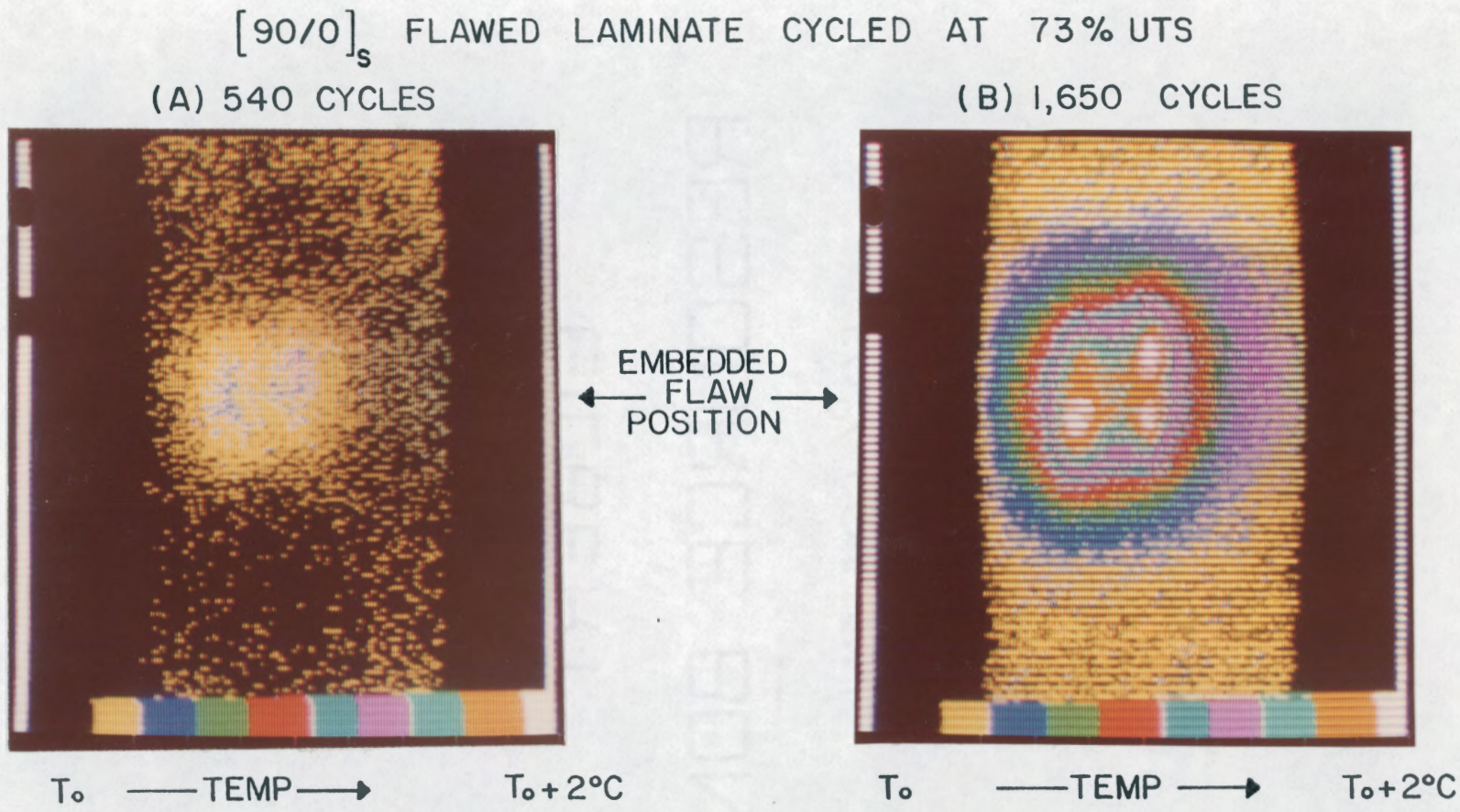

Fig. 17. Heat pattern of a type 4 $[90/0]_s$ flawed laminate under cyclic loading at 73% UTS. The maximum nominal axial stress in the 0 degree plies is 130% of the notched tensile strength of type 1 specimens. (A) 540 cycles; (B) 1,650 cycles; (C) 1,900 cycles; and (D) 10,000 cycles.

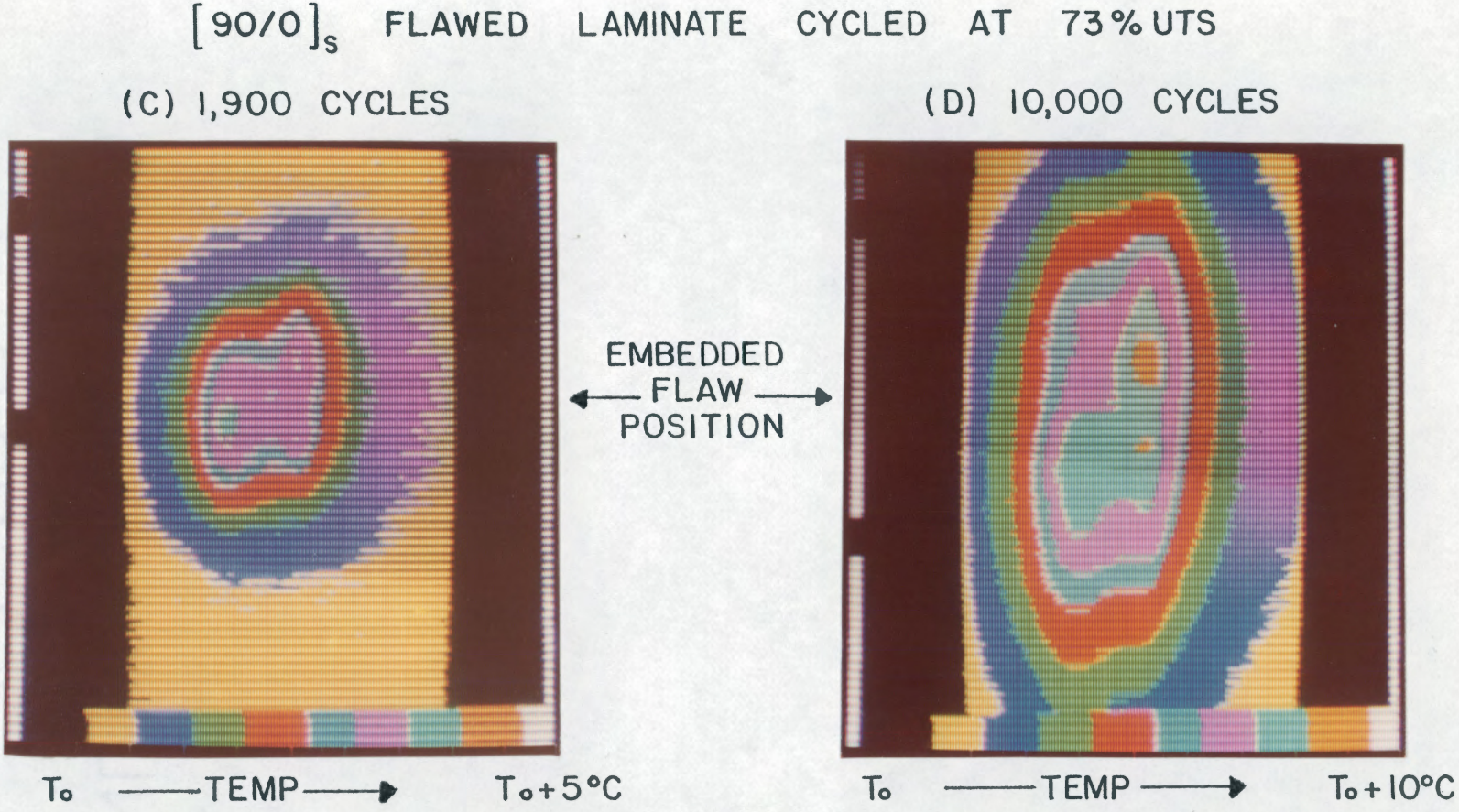

Fig. 17. Heat pattern of a type 4 $[90/0]_s$ flawed laminate under cyclic loading at 73% UTS. The maximum nominal axial stress in the 0 degree plies is 130% of the notched tensile strength of type 1 specimens. (A) 540 cycles; (B) 1,650 cycles; (C) 1,900 cycles; and (D) 10,000 cycles.

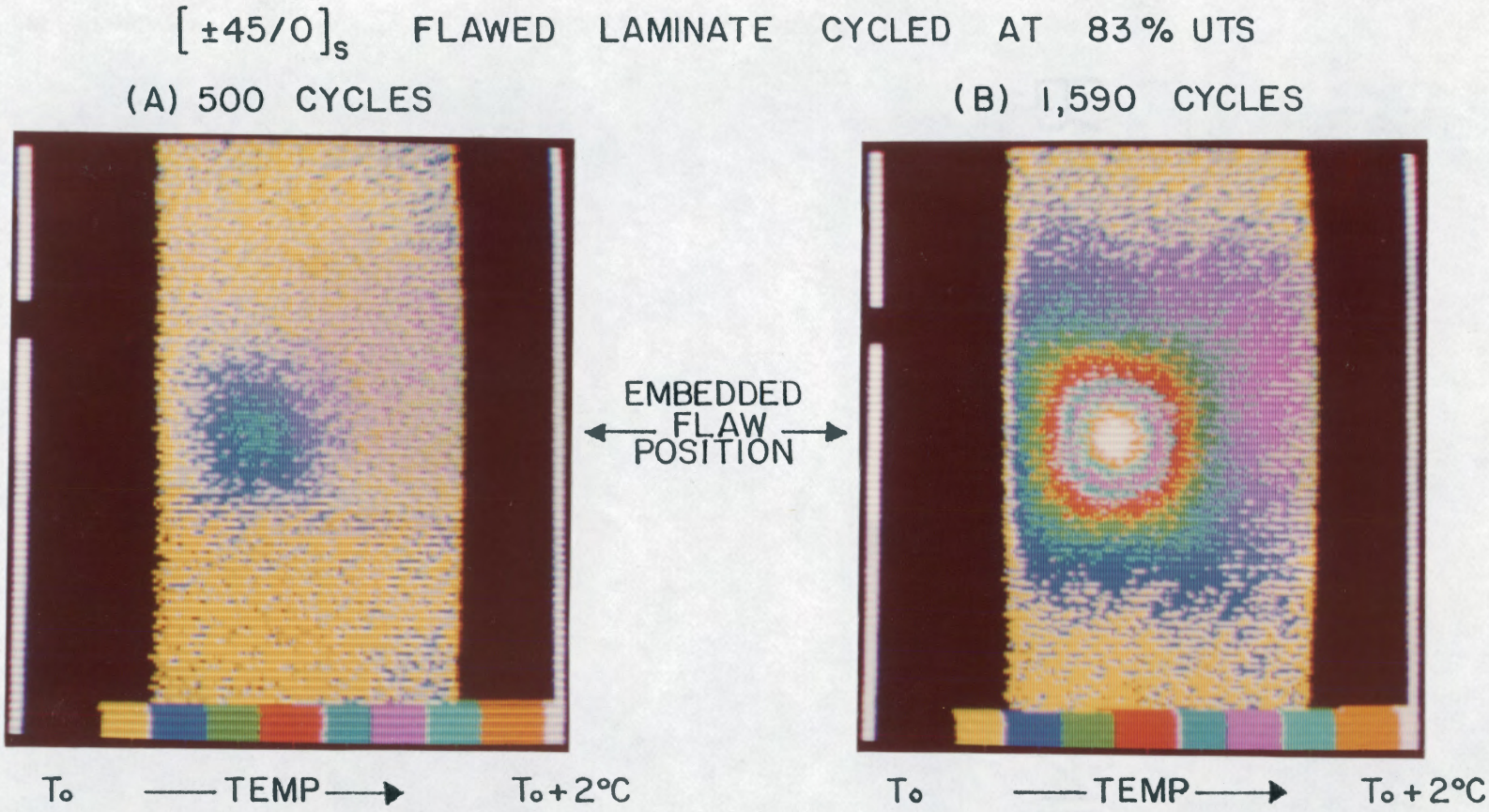

Fig. 18. Heat pattern of a type 6 $[\pm 45/0]_s$ flawed laminate under cyclic loading at 83% UTS. The maximum nominal axial stress in the 0 degree plies is 130% of the notched tensile strength of type 1 specimens. (A) 500 cycles; (B) 1,590 cycles; (C) 2,140 cycles; and (D) 8,200 cycles.

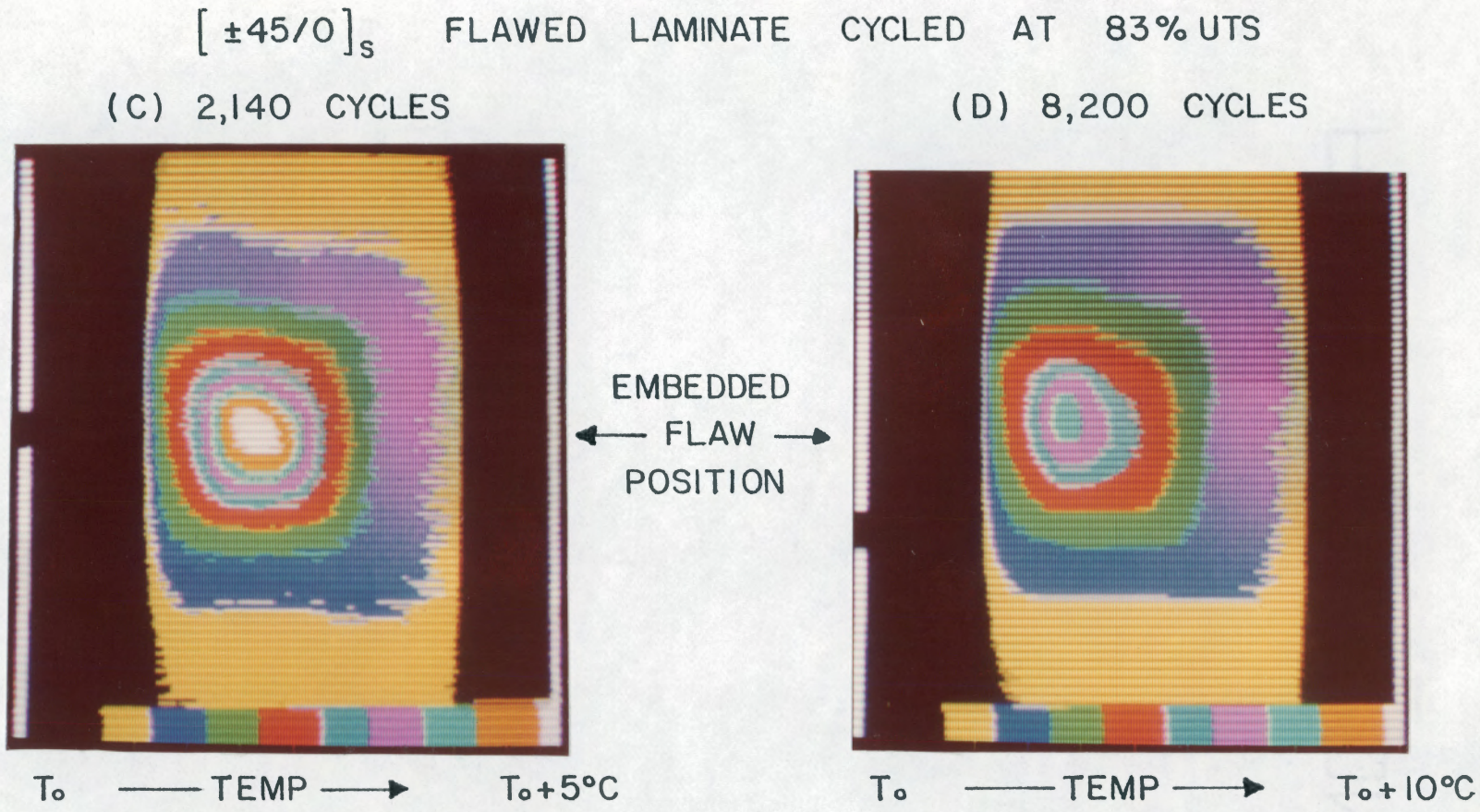

Fig. 18. Heat pattern of a type 6 $[\pm 45/0]_s$ flawed laminate under cyclic loading at 83% UTS. The maximum nominal axial stress in the 0 degree plies is 130% of the notched tensile strength of type 1 specimens. (A) 500 cycles; (B) 1,590 cycles; (C) 2,140 cycles; and (D) 8,200 cycles.

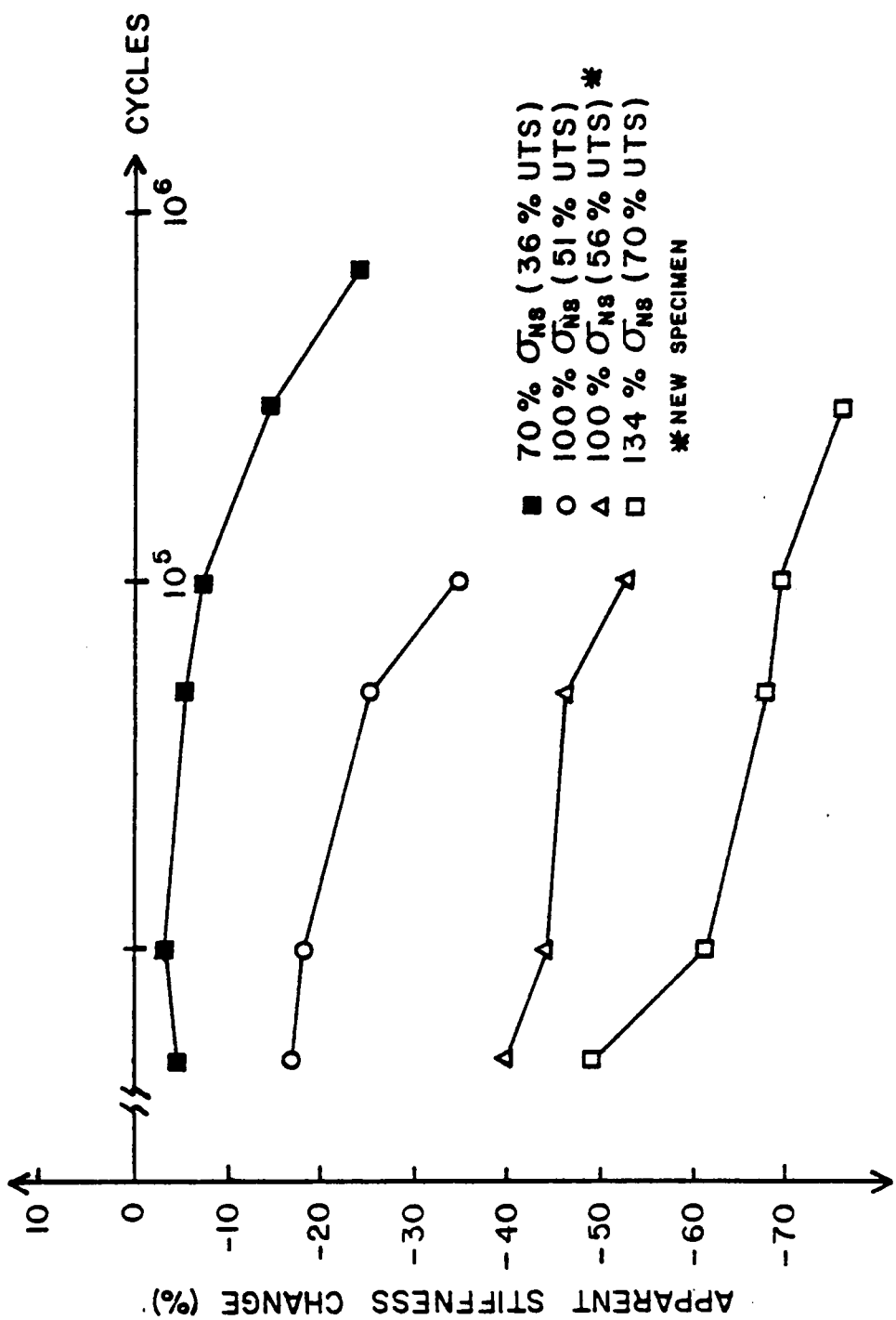

Fig. 19. Changes in the apparent stiffness across the flawed region of type 4 $[90/0]_s$ flawed laminates during fatigue loading.

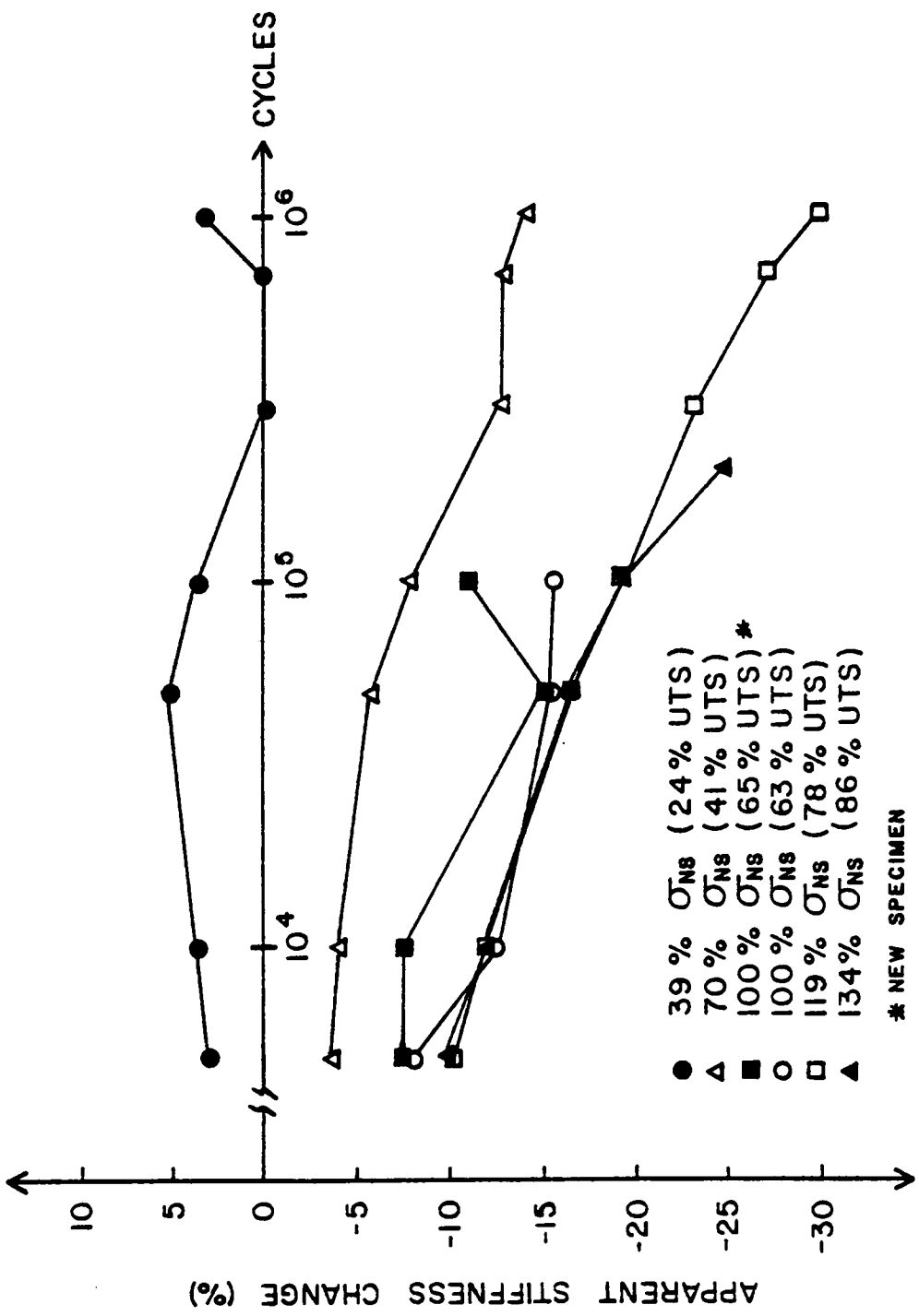

Fig. 20. Changes in the apparent stiffness across the flawed region of type 6 $[\pm 45/0]_S$ flawed laminates during fatigue loading.

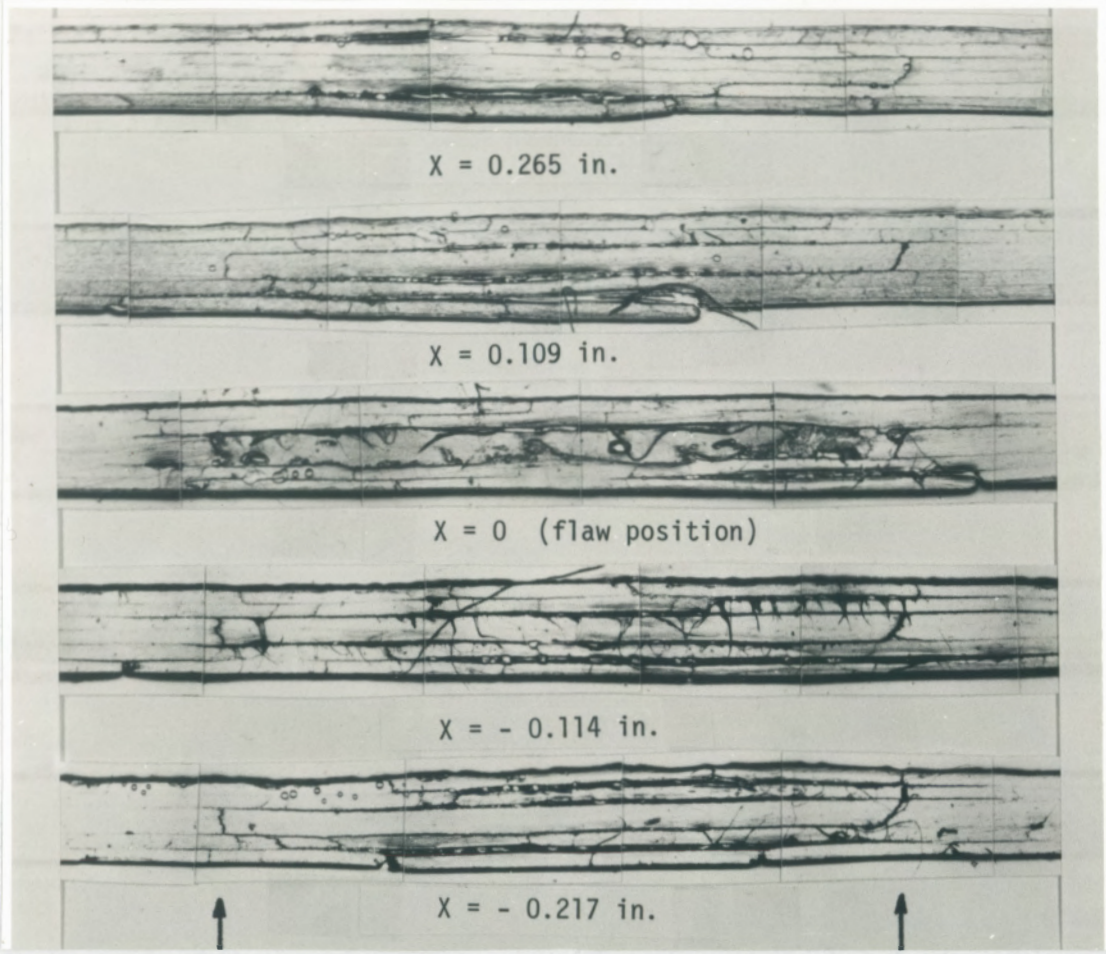

Fig. 21. Sectioning replicas of a type 6 $[\pm 45/0]_s$ laminate with a transverse notch embedded in the interior 0 deg. plies, after 200,000 cycles of fatigue loading at 85% UTS. The nominal axial stress in the 0 degree plies is 134% of the notched tensile strength of type 1 specimens.

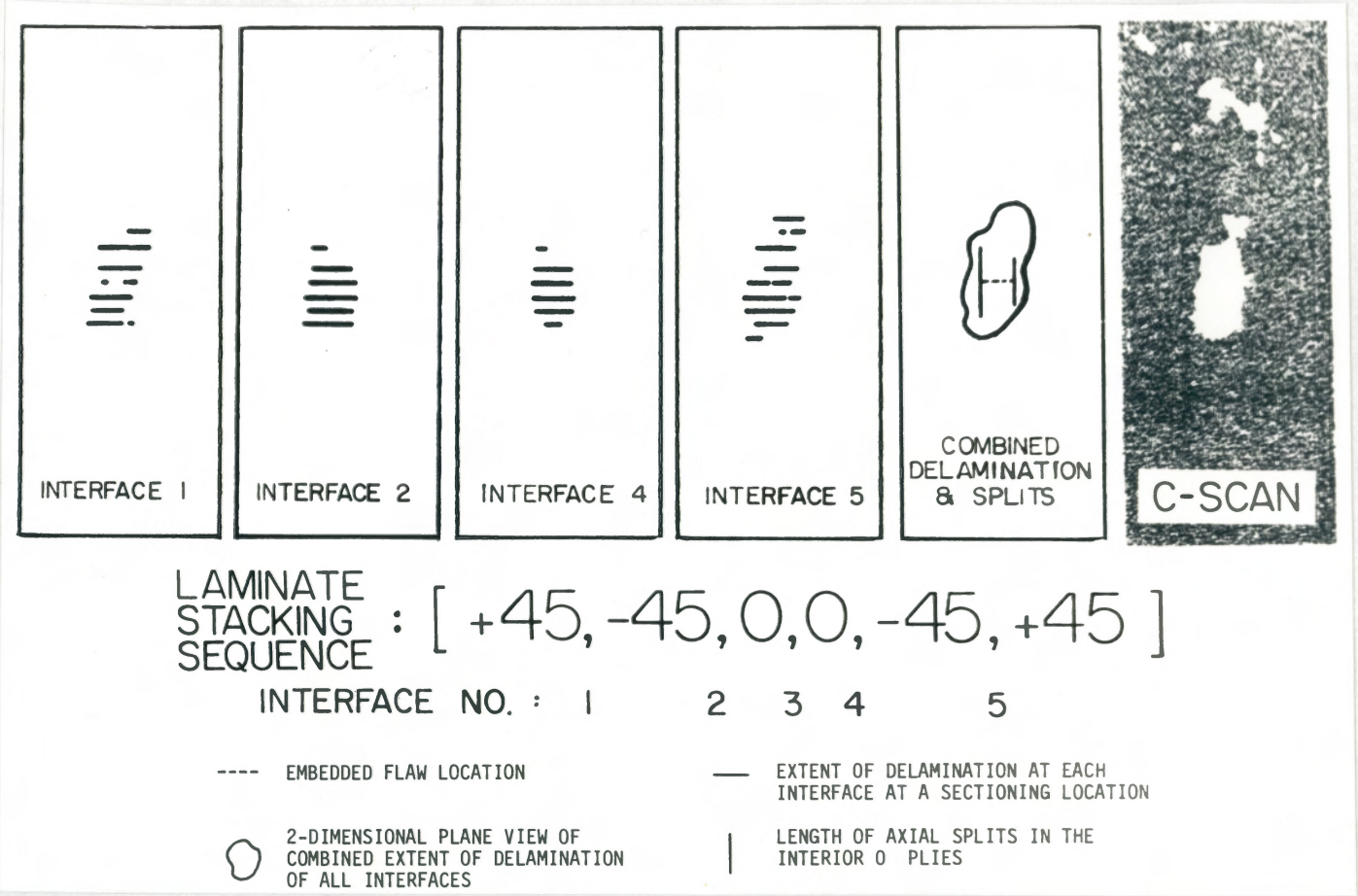

Fig. 22. Results of sectioning studies on a type 6 $[45/0]_s$ flawed laminate after 200,000 cycles of fatigue loading at 85% UTS. (A) +45/-45 interface; (B) -45/0 interface; (C) 0/-45 interface; (D) -45/+45 interface; (E) combined diagram of delamination and axial splits in the interior 0 degree plies; and (F) ultrasonic c-scan of the specimen.

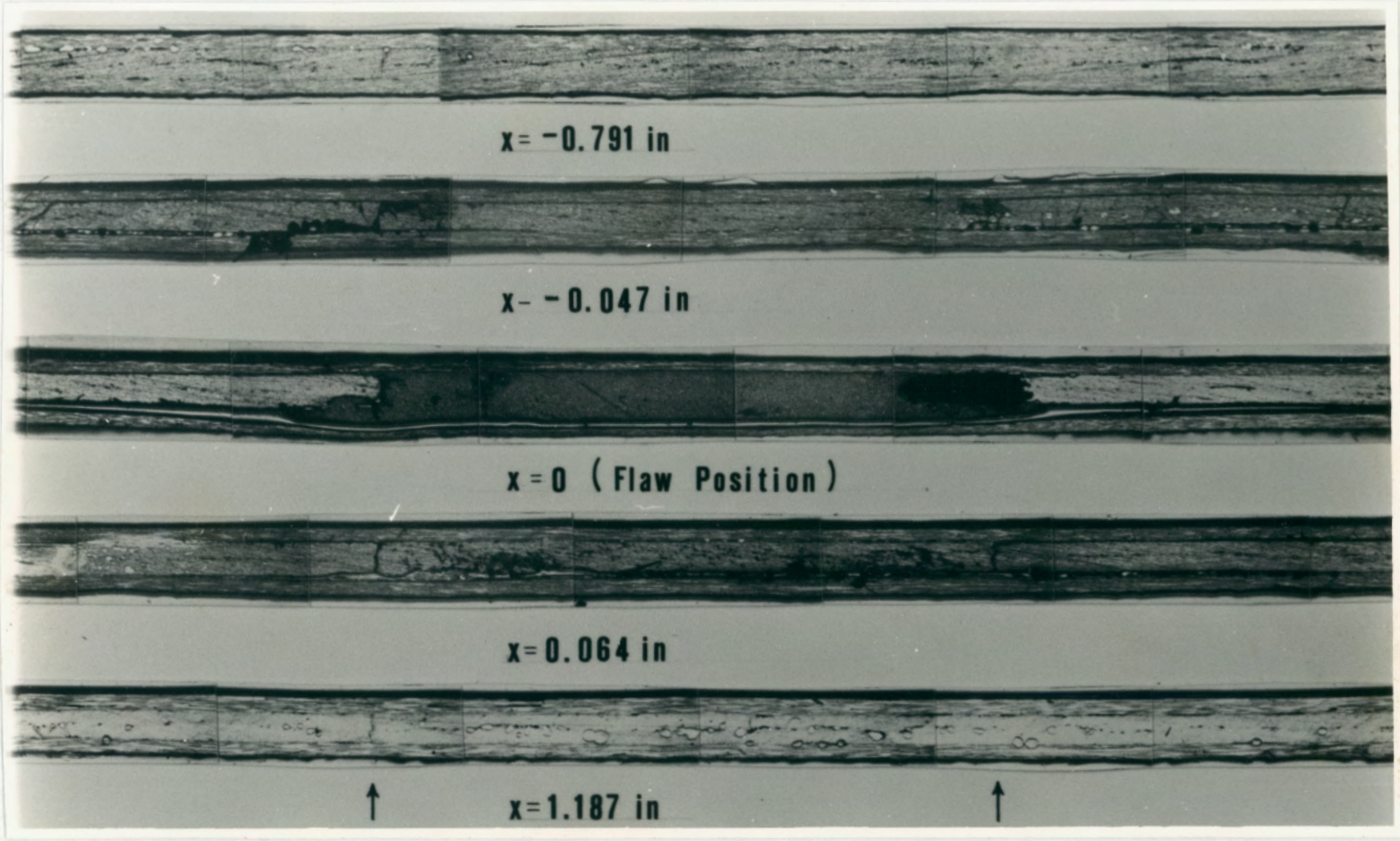

Fig. 23. Sectioning replicas of a type 4 $[90/0]_s$ laminate with a transverse notch in the interior 0 degree plies after 100,000 cycles of fatigue loading at 51% UTS. The nominal axial stress in the 0 degree plies is 100% of the notched tensile strength of type 1 specimens.

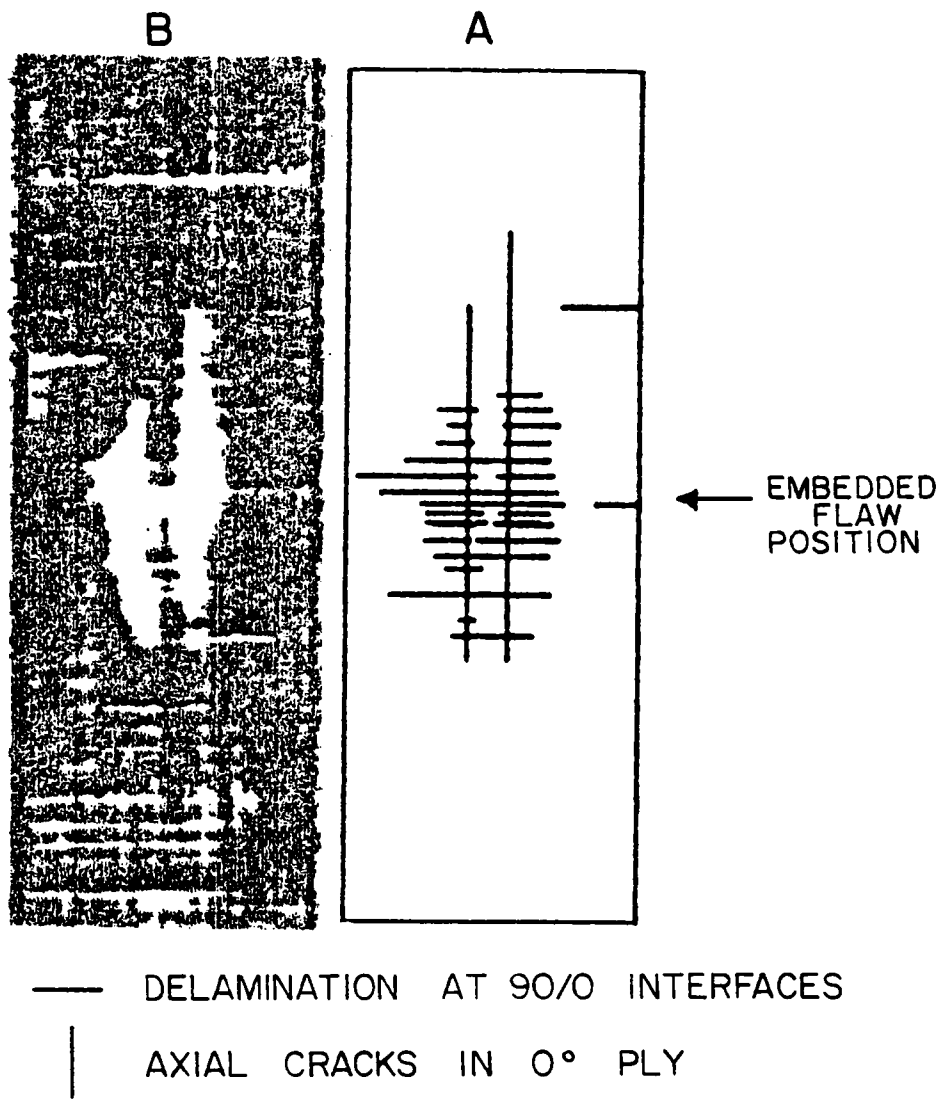

Fig. 24. Results of sectioning studies on a type 4 $[90/0]_s$ flawed laminate after 100,000 cycles of fatigue loading at 51% UTS. (A) delamination of 90/0 interfaces and axial splits in the interior 0 degree plies; and (B) ultrasonic c-scan of the specimen.

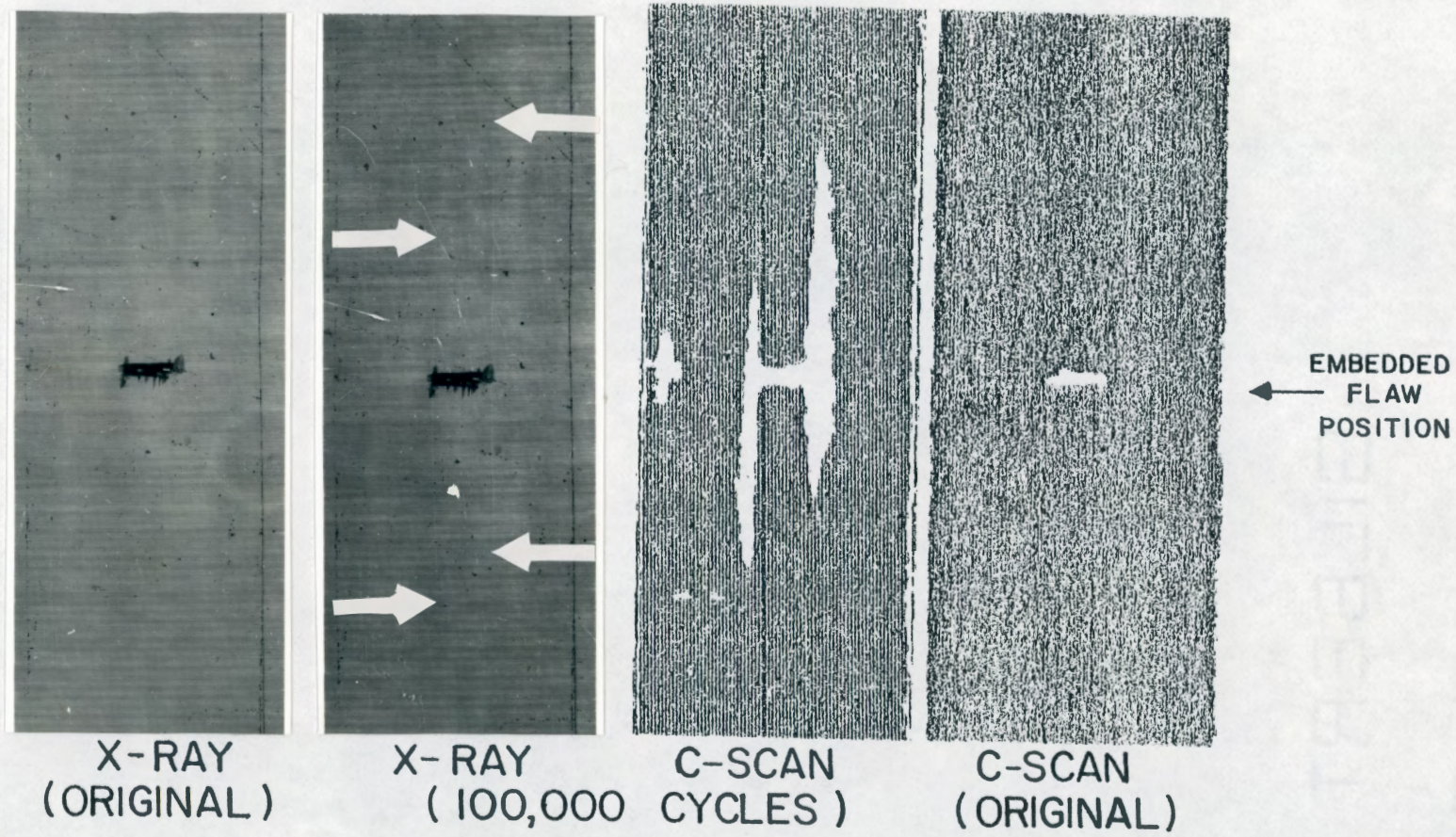

Fig. 25. X-ray radiographs and ultrasonic c-scans of a type 4 $[90/0]_S$ flawed laminate after 100,000 cycles of fatigue loading at 55% UTS. The nominal axial stress in the 0 degree plies is 100% of the notched tensile strength of type 1 specimens.

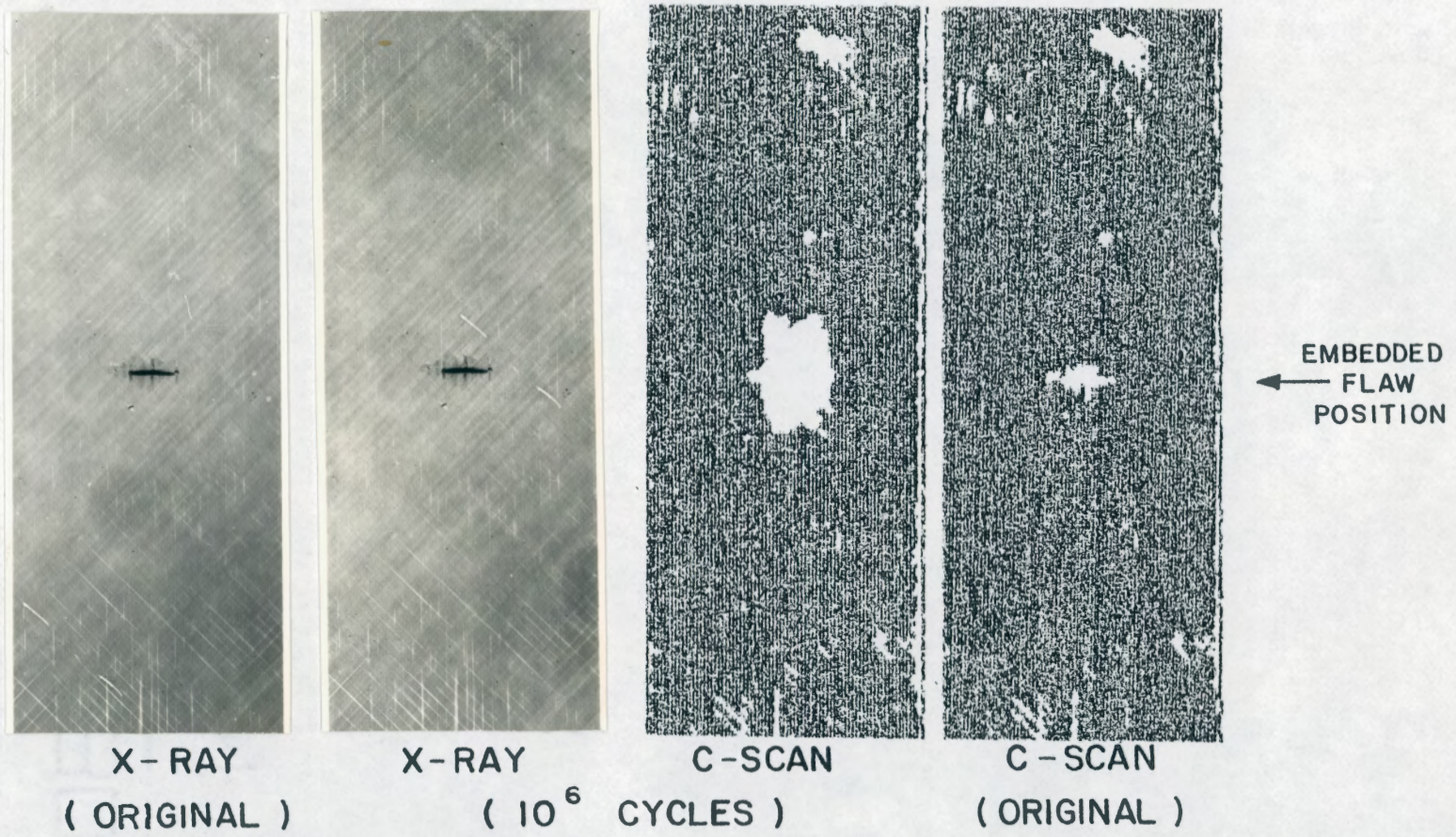

Fig. 26. X-ray radiographs and ultrasonic c-scans of a type 6 $[\pm 45/0]_S$ flawed laminate after one million cycles of fatigue loading at 78% UTS. The nominal axial stress in the 0 degree plies is 120% of the notched tensile strength of type 1 specimens.

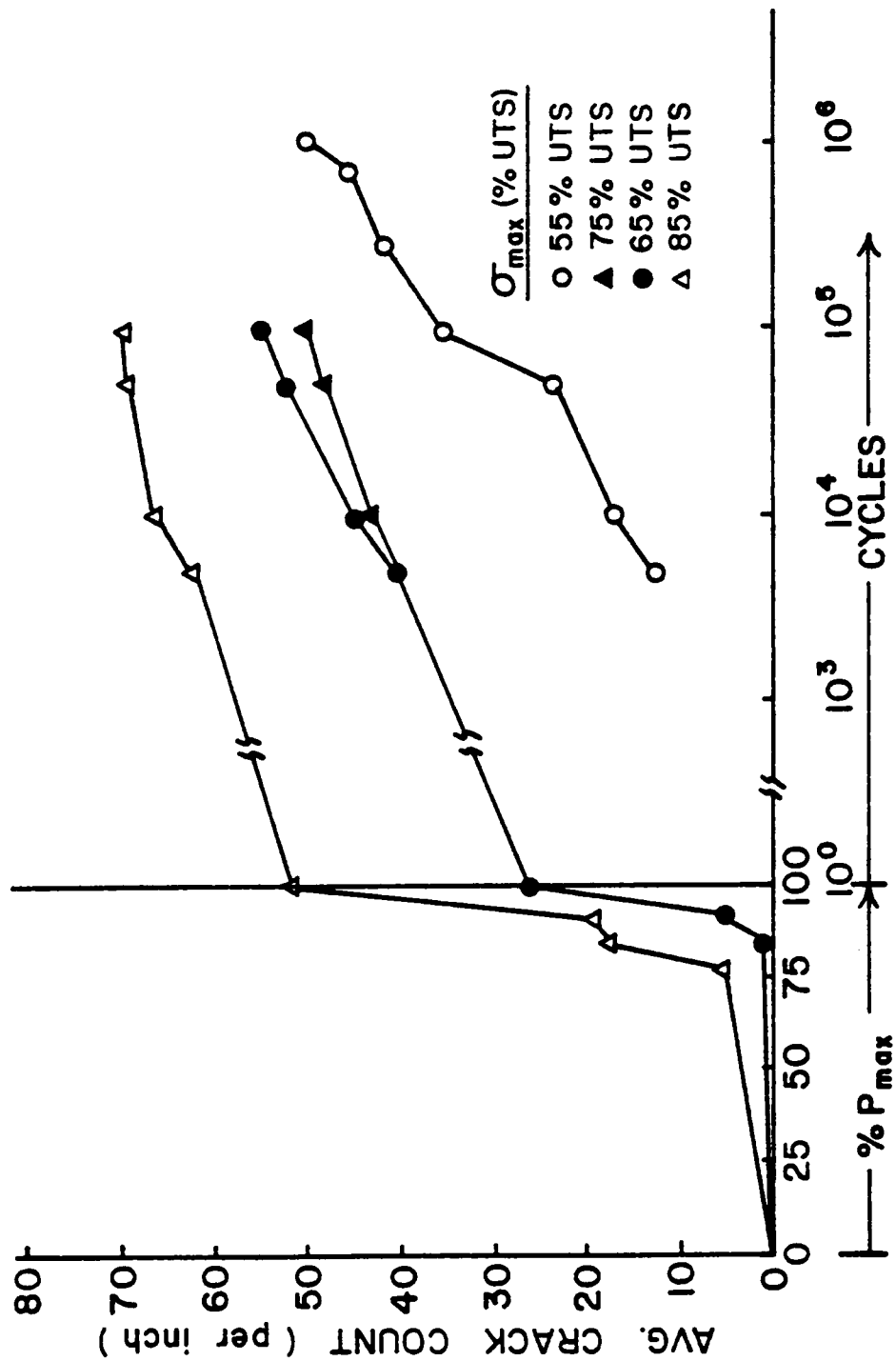

Fig. 27. Transverse crack formation in the 90 degree plies of the type 3 $[0/90]_s$ flawed laminates under static and fatigue loading.

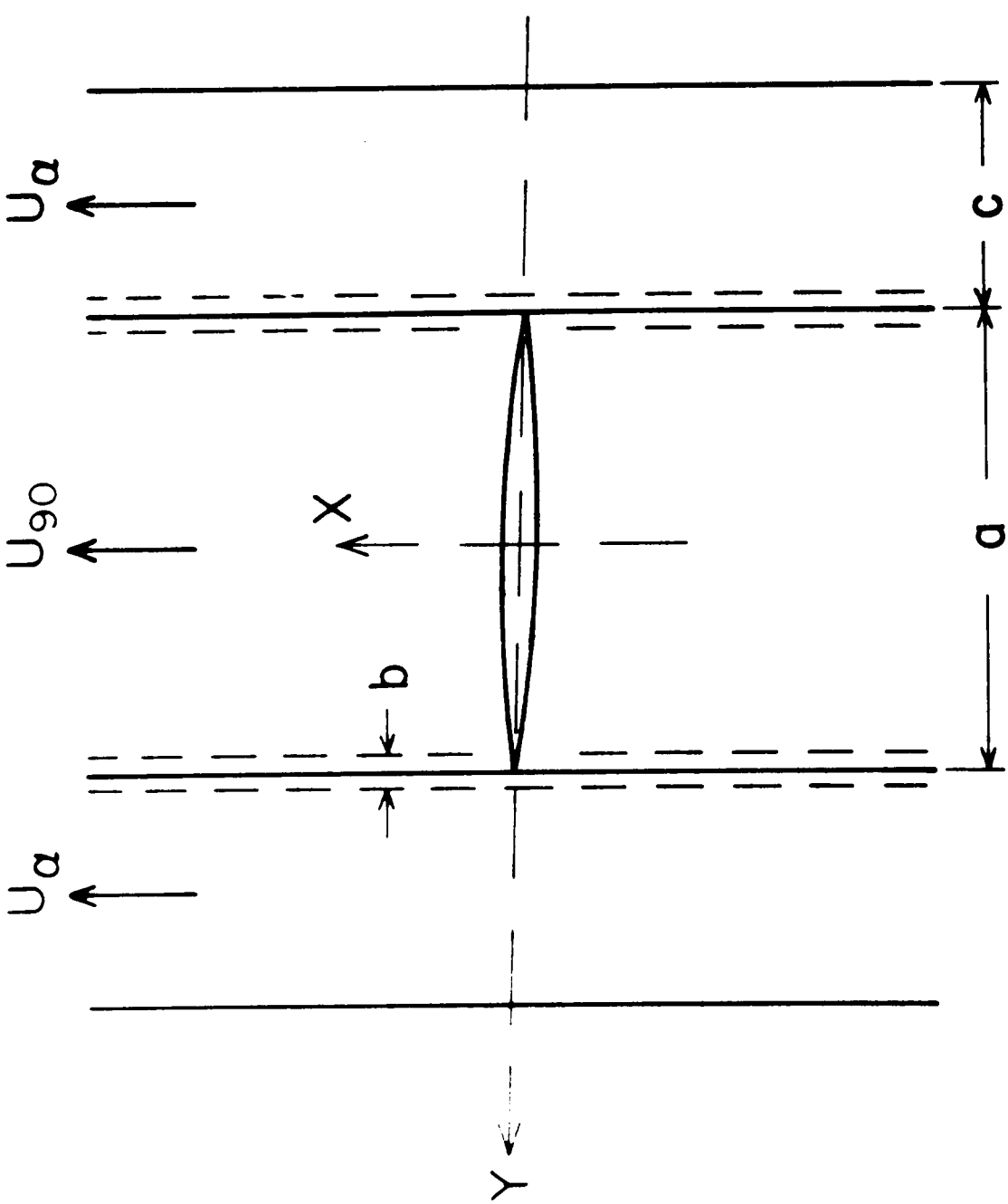

Fig. 28. Schematic diagram of a crack in two 90 degree plies at the edge of a laminate (from reference 26).

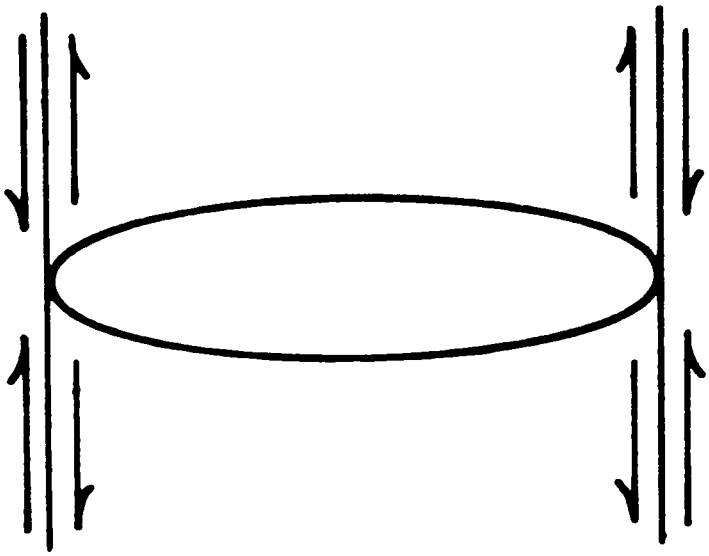

A

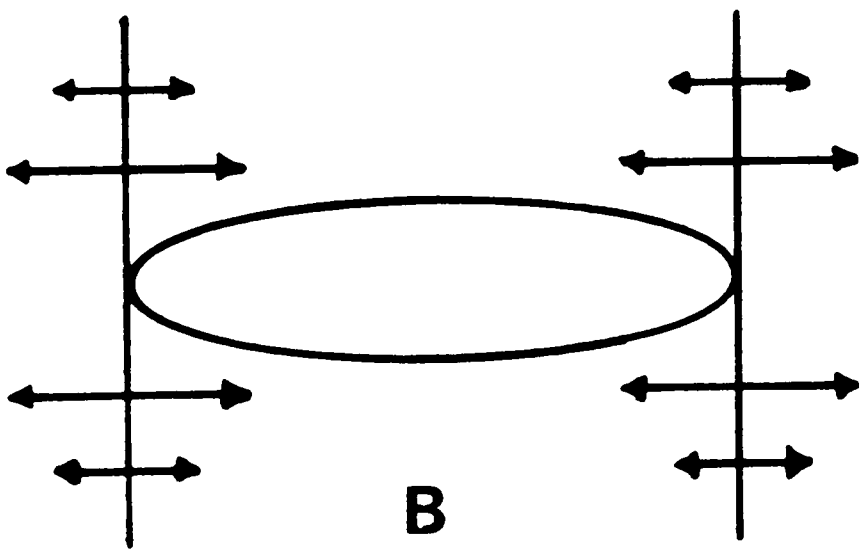

B

Fig. 29. Two basic modes of degradation at a notch in a unidirectional lamina.

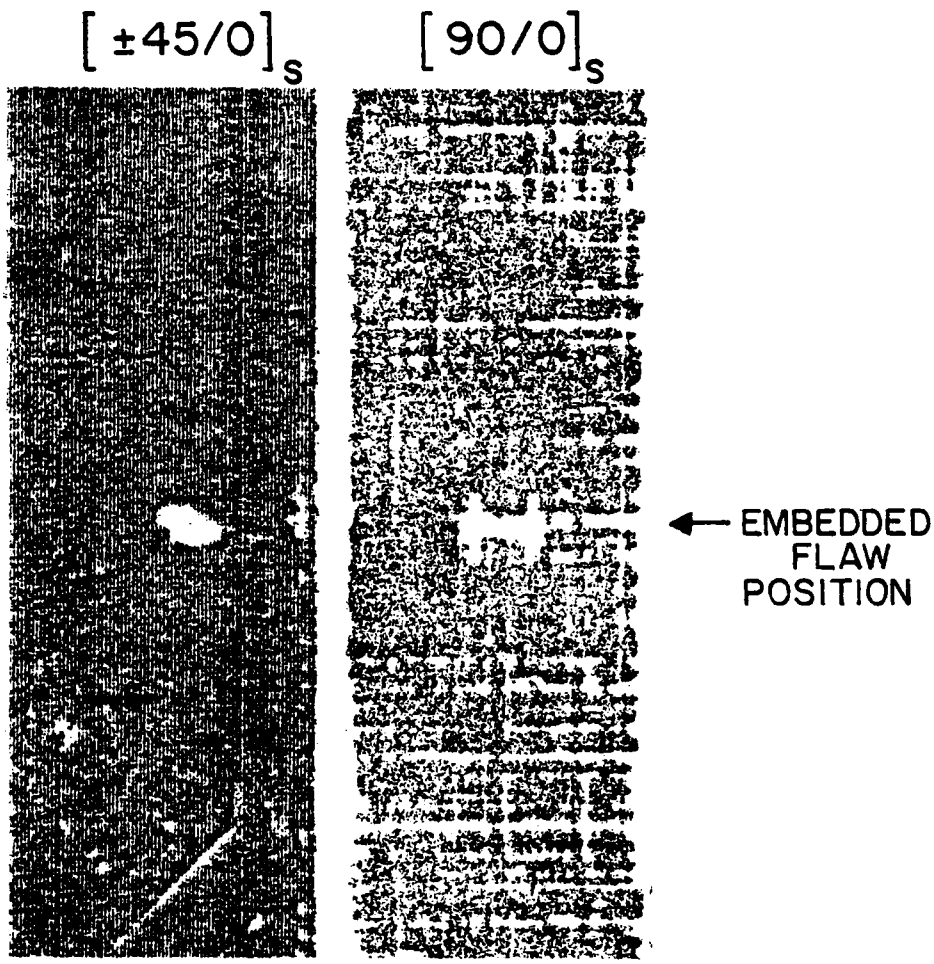

Fig. 30. Ultrasonic c-scans of a type 4 $[90/0]_s$ and a type 6 $[\pm 45/0]_s$ flawed laminate after 100,000 cycles of fatigue loading. In each case, the nominal axial stress in the interior 0 degree plies is 70% of the notched tensile strength of type 1 specimens.

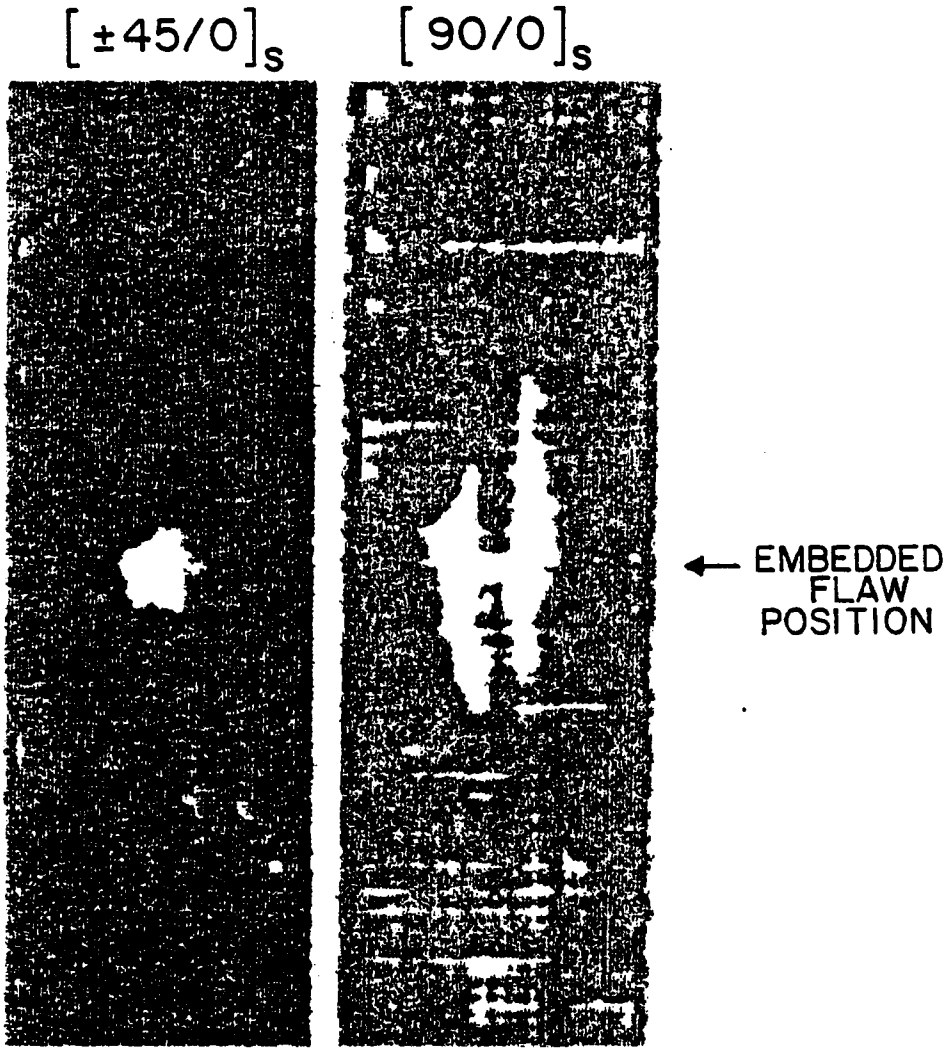

Fig. 31. Ultrasonic c-scans of a type 4 $[90/0]_s$ and a type 6 $[\pm 45/0]_s$ flawed laminate after 100,000 cycles of fatigue loading. In each case, the nominal axial stress in the interior 0 degree plies is 100% of the notched tensile strength of type 1 specimens.

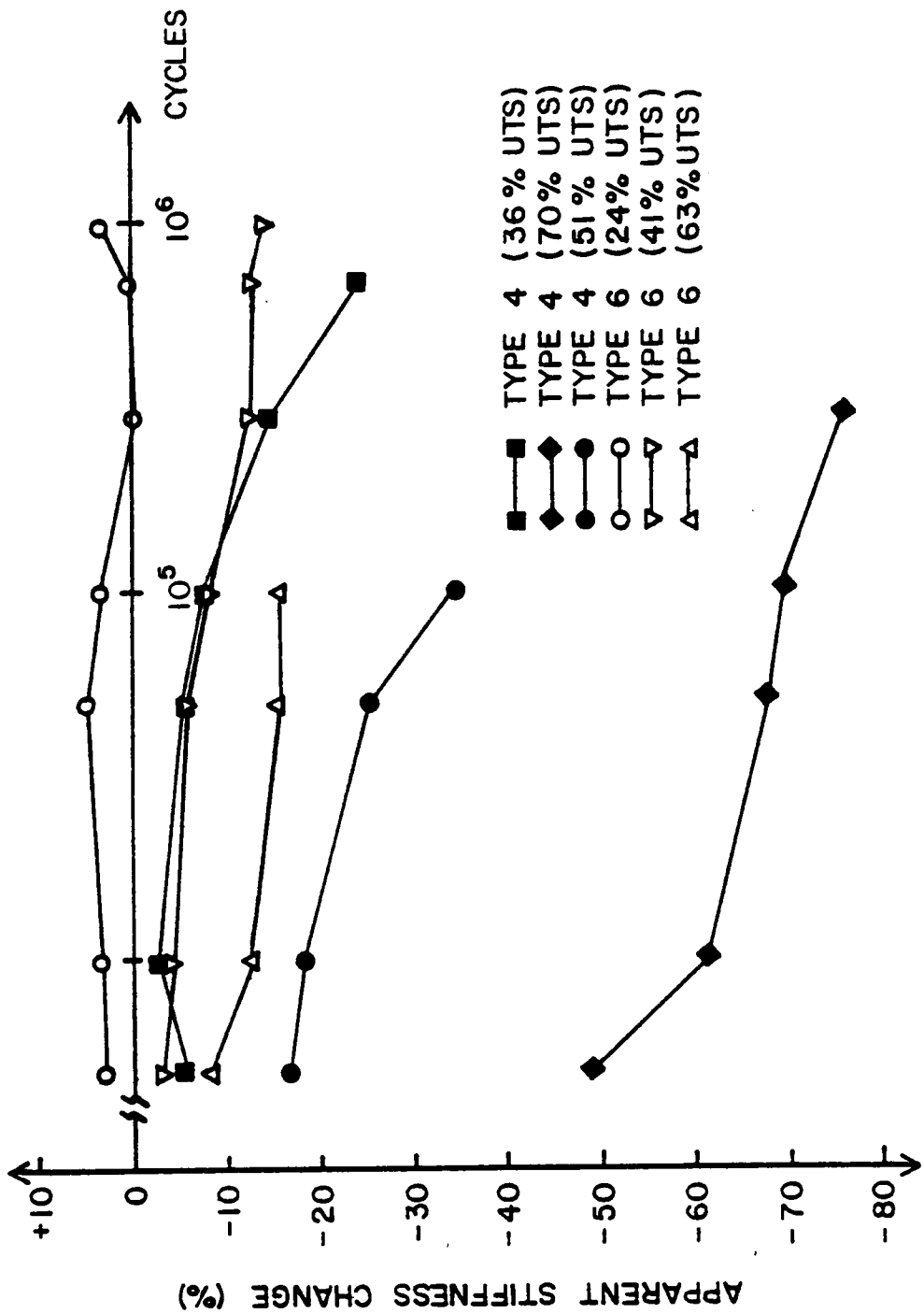

Fig. 32. Changes in the apparent stiffness across the flawed region of type 4 $[90/0]_s$ and type 6 $[\pm 45/0]_s$ flawed laminates during fatigue loading.

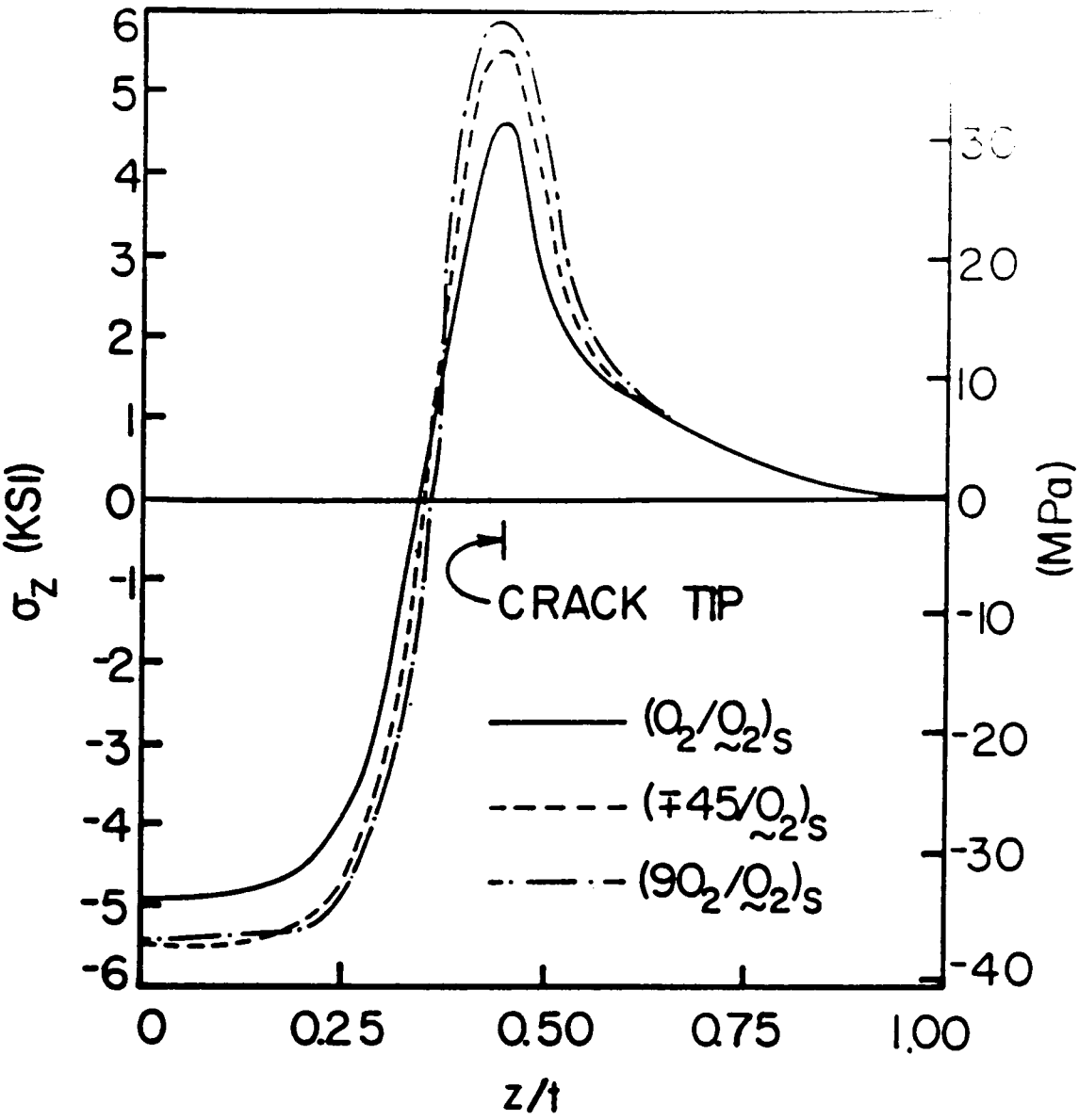

Fig. 33. Constraint effect on the through-the-thickness interlaminar normal stress distribution (from reference 27).

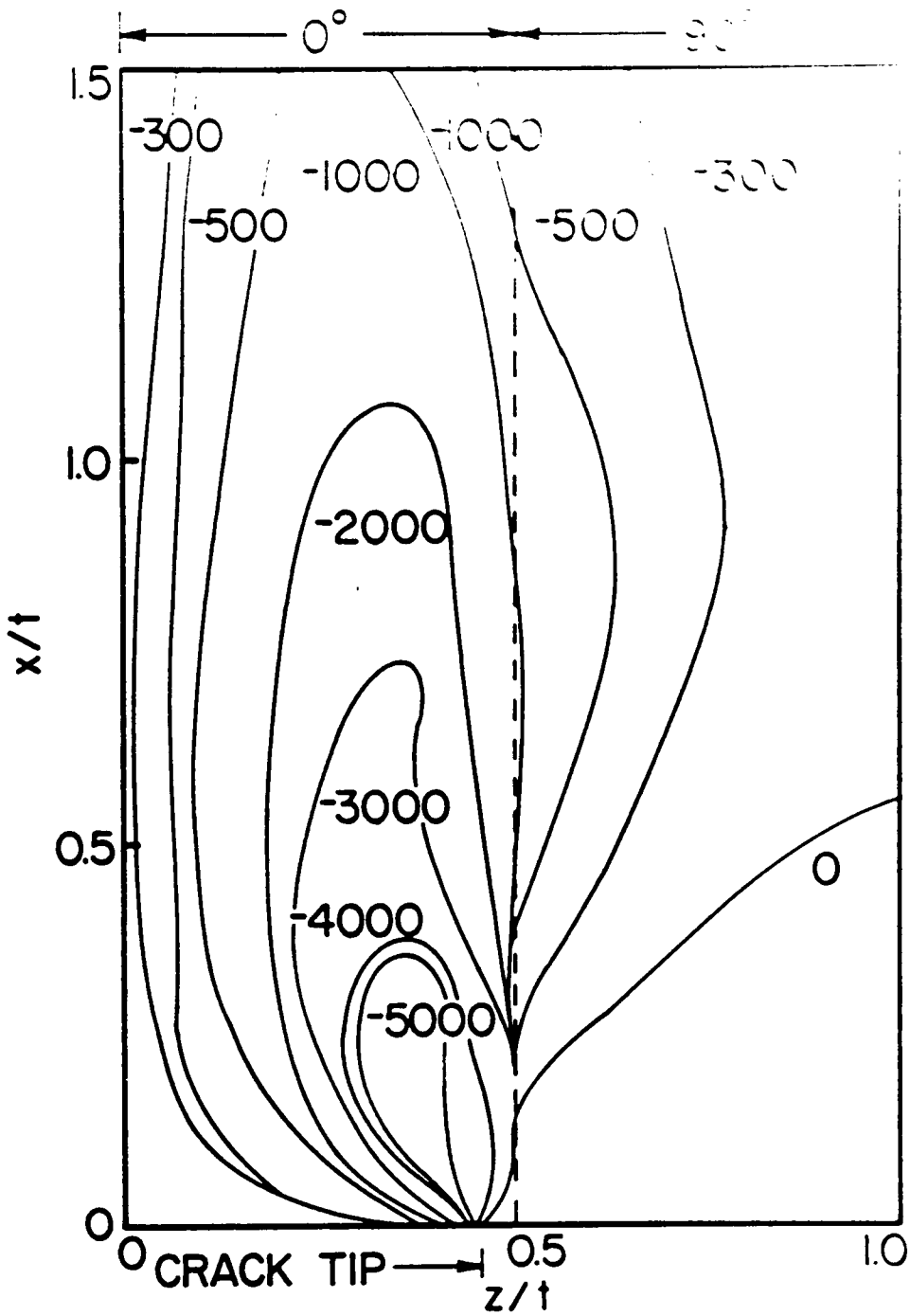

Fig. 34. Contours of τ_{xz} (psi) for a $[90_2/0_2]_s$ laminate with 0 degree ply damage (from reference 27).

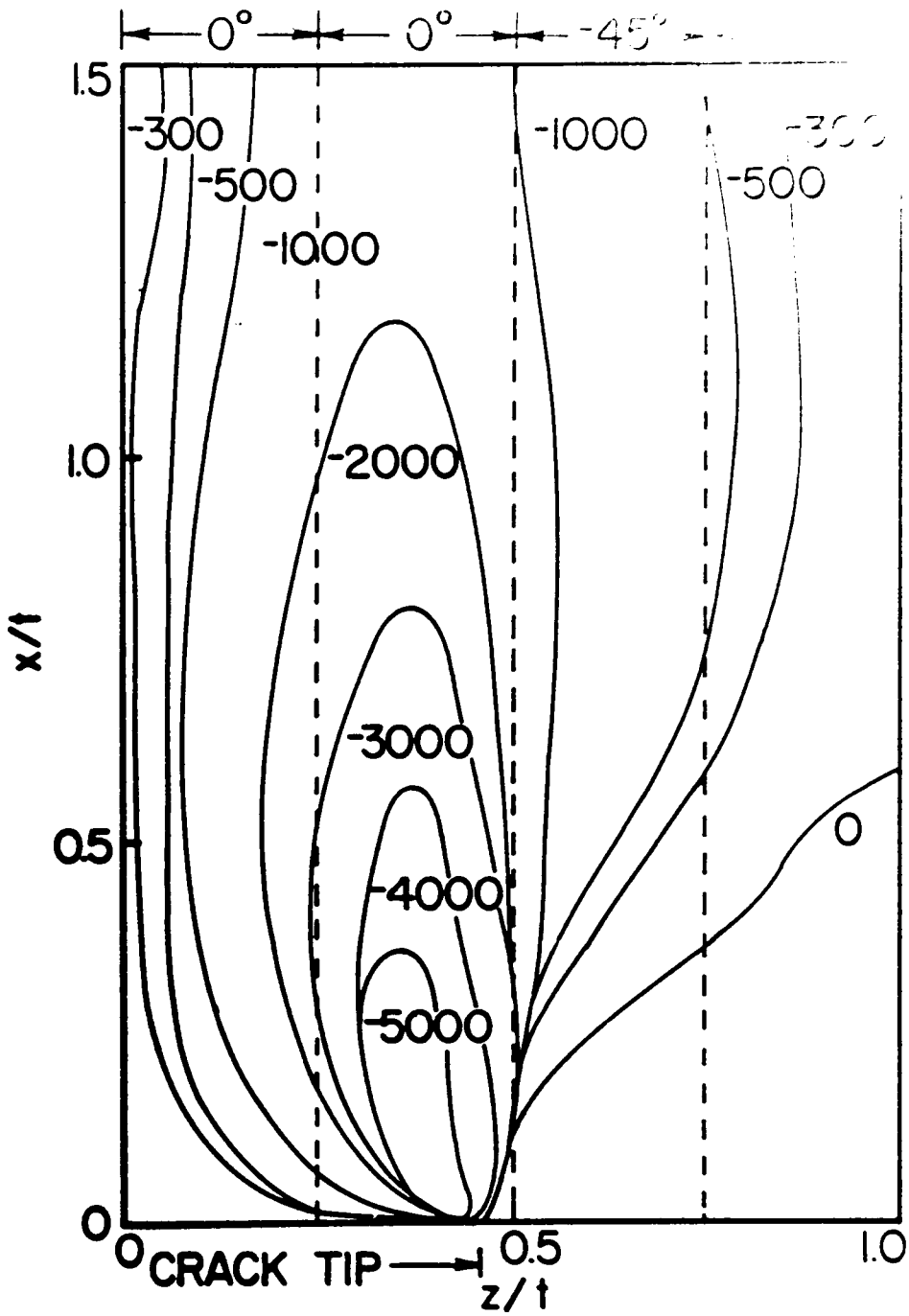

Fig. 35. Contours of τ_{xz} (psi) for a $[\pm 45/0_2]_s$ laminate with 0 degree ply damage (from reference 27).

The vita has been removed from the scanned document

INVESTIGATION OF CONSTRAINT EFFECTS ON FLAW GROWTH IN COMPOSITE LAMINATES

by

Peter Chun-Ngok Yeung

(ABSTRACT)

An investigation was conducted to study the constraint effects on flaw growth in composite laminates. Results were presented for the case of a transverse flaw in an interior ply perpendicular to the loading axis. Two orientations of the flawed ply were examined (0 and 90 degrees), and two distinctly different constraint situations were studied (cross-ply constraint and biaxial constraint).

Throughout the study, various nondestructive testing methods were employed to evaluate the material response and to determine the damage and damage growth in the specimens. These techniques include replication, ultrasonic c-scan, ultrasonic attenuation, acoustic emission, x-radiography, thermography and stiffness measurement.

The effects of constraint on the response of composite materials can be classified in two categories: (a) in-plane effects and (b) through-the-thickness effects. In-plane constraint is the principal contributor to notched strength and changes in notched strength under quasi-static loading. Through-the-thickness constraint controls the pattern and spacing of transverse cracks in the off-axis plies to form a characteristic damage state in the laminates. Out-of-plane stresses produced by constraints are influential on the growth of damage along ply interfaces, especially during cyclic loading.

The mode of damage and the extent of damage in constrained notched

plies are governed by the stress state in those plies, as determined by the constraining plies, and the relationship of the stress state to the strength state. Maximum constraint on the flawed ply does not produce minimum damage in the laminate; and the lesser degree of damage (in terms of axial splitting and delamination) does not necessarily result in a higher laminate strength or long fatigue lifes. In the design of composite structures, a compromise has to be reached with regard to optimizing material parameters such as strength, stiffness, fatigue life and residual strength. In maximizing one parameter, one might have to sacrifice other requirements on the other material properties in the design.